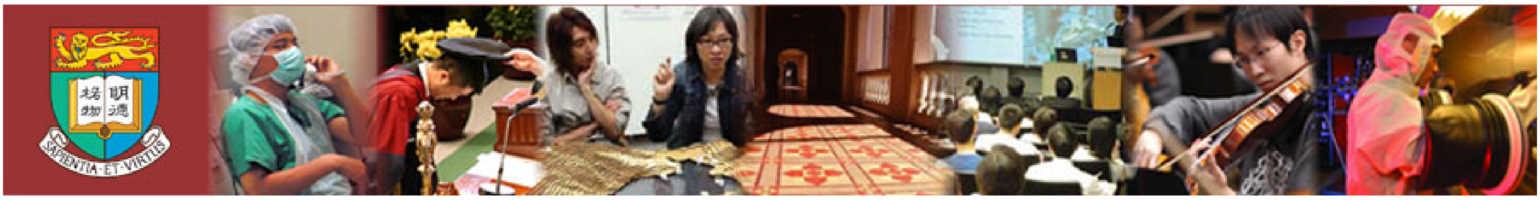

Title	Tectonic affinity of the west Qinling terrane (central China): North China or Yangtze?
Author(s)	Zheng, JP; Griffin, WL; Sun, M; O'Reilly, SY; Zhang, HF; Zhou, HW; Xiao, L; Tang, HY; Zhang, ZH
Citation	Tectonics, 2010, v. 29 n. 1, article no. TC2009
Issued Date	2010
URL	http://hdl.handle.net/10722/159506
Rights	Tectonics. Copyright © American Geophysical Union.

TECTONICS, VOL. 29, TC2009, doi:10.1029/2008TC002428, 2010

Tectonic affinity of the west Qinling terrane (central China): North China or Yangtze?

J. P. Zheng,[1,2] W. L. Griffin,[3] M. Sun,[4] S. Y. O'Reilly,[3] H. F. Zhang,[1] H. W. Zhou,[1] L. Xiao,[1] H. Y. Tang,[1] and Z. H. Zhang[1]

Received 24 November 2008; revised 28 August 2009; accepted 6 October 2009; published 1 April 2010.

[1] Our ignorance about the tectonic affinity of the western Qinling-Songpan-Ganzi tectonic region, which is strategically located between the northeastern corner of the Tibetan Plateau, the northwestern corner of the Yangtze block, and the southwestern corner of the north China block, limits our understanding of the tectonic evolution of east Asia. Basaltic volcanic rocks in the Duofutun area within the west Qinling terrane in Qinghai Province (China), the northernmost part of the Songpan-Ganzi region, contain coeval magmatic zircons that constrain the eruption age of the host basalts to ~14 Ma. More significantly, the basalts have entrained zircon xenocrysts from the deep crust that record the presence of unexposed Neoarchean (2.7–2.5 Ga) basement. U-Pb and Hf isotope data from the xenocrysts reveal that this basement has undergone a complex evolution that includes the addition of new mantle-derived material at ~2.7–2.4 and 1.1–0.8 Ga and crustal reworking events at ~1.8 and 1.4 Ga. Phanerozoic thermal events at 320–300, 230, and 160 Ma have also modified (reworked) the basement. Using these data, we interpret at least the western part of the west Qinling orogenic terrane as a microcontinental block that originally separated from the north China block, closed with the northern Yangtze block during the Meso-Neoproterozoic, and then redocked with the southern part of the north China block in the Phanerozoic (i.e., early Paleozoic). The west Qinling terrane was then affected by the northward subduction and collision of the Yangtze block in the Paleozoic and early Mesozoic and underwent lithospheric extension in Jurassic time. **Citation:** Zheng, J. P., W. L. Griffin, M. Sun, S. Y. O'Reilly, H. F. Zhang, H. W. Zhou, L. Xiao, H. Y. Tang, and Z. H. Zhang (2010), Tectonic affinity of the west Qinling terrane (central China): North China or Yangtze?, *Tectonics*, *29*, TC2009, doi:10.1029/2008TC002428.

[1]State Key Lab of Geological Processes and Mineral Resources, China University of Geosciences, Wuhan, China.

[2]Also at Guilin University of Technology, Guilin, China

[3]Australian Research Council National Key Centre for Geochemical Evolution and Metallogeny of Continents, Department of Earth and Planetary Sciences, Macquarie University, Sydney, New South Wales, Australia.

[4]Department of Earth Sciences, University of Hong Kong, Hong Kong, China.

0278-7407/10/2008TC002428

1. Introduction

[2] The Qinling orogen separates the north China block from the south China block and links the Kunlun and Qilian orogens to the west, with the Dabie-Sulu orogen to the east (Figures 1a and 1b). These terranes make up an important tectonic zone in eastern Asia [*Zhang et al.*, 1995, 1996, 2004; *Meng and Zhang*, 2000; *Ratschbacher et al.*, 2003]. The Qinling orogen can be roughly divided into eastern (east Qinling) and western (west Qinling) segments, taking the Baoji-Chengdu Railway as a boundary [*Zhang et al.*, 1995, 1996]. East Qinling can be further subdivided into south and north Qinling. It is commonly accepted that northward subduction of oceanic crust beneath the southern margin of the north China block along the Shangdan suture started during the Ordovician, and closure and collapse of the associated back-arc system and collision of the south China block during Middle Devonian time resulted in the north Qinling orogen [*Kröener et al.*, 1993; *Zhang et al.*, 1994; *Lerch et al.*, 1995; *Cui et al.*, 1995; *Xue et al.*, 1996]. Synchronous with Devonian back-arc collapse, rifting split off part of the south China block, leaving its northernmost segment, known as the south Qinling microcontinent, attached to north Qinling/north China block [*Lai et al.*, 1992]. West Qinling tectonically forms the northernmost part of the western Qinling-Songpan-Ganzi region [*Zhang et al.*, 2004] situated in central China (Figures 1a and 1b); this region is important for understanding the tectonic evolution of China, but little is known because of the complex deformation and tectonic modification of the area. Undoubtedly, the deep lithospheric structure (i.e., the nature of the basement) is important, not only to understand the evolution of the Qinling orogen but also to elucidate the tectonic history of the Tibetan Plateau and eastern Asia.

[3] Basaltic rocks, representing asthenosphere-derived magmas, can be used as natural "drill holes" to sample the deep lithosphere. In addition to magmatic zircons that allow the dating of the magma's eruption, basaltic rocks can also contain entrained xenocrystic zircons derived from disaggregated xenoliths, and these xenocrysts may record the history of the unexposed deep lithosphere. Recent studies of zircons in xenoliths and zircon xenocrysts from several regions in China (Figure 1a) have shown that the deep crust may be significantly older than the exposed upper crust, for example, in the Xinyang area of the north China block [*Zheng et al.*, 2004a]; the Jingshan, Ningxiang, and Zhenyuan areas of the Yangtze block [*Zheng et al.*, 2006a]; and the Pingle and Pingnan areas of the west Cathaysia block [*Zheng et al.*, 2008a]. In order to determine if a similar scenario may apply to the west Qinling orogenic terrane,

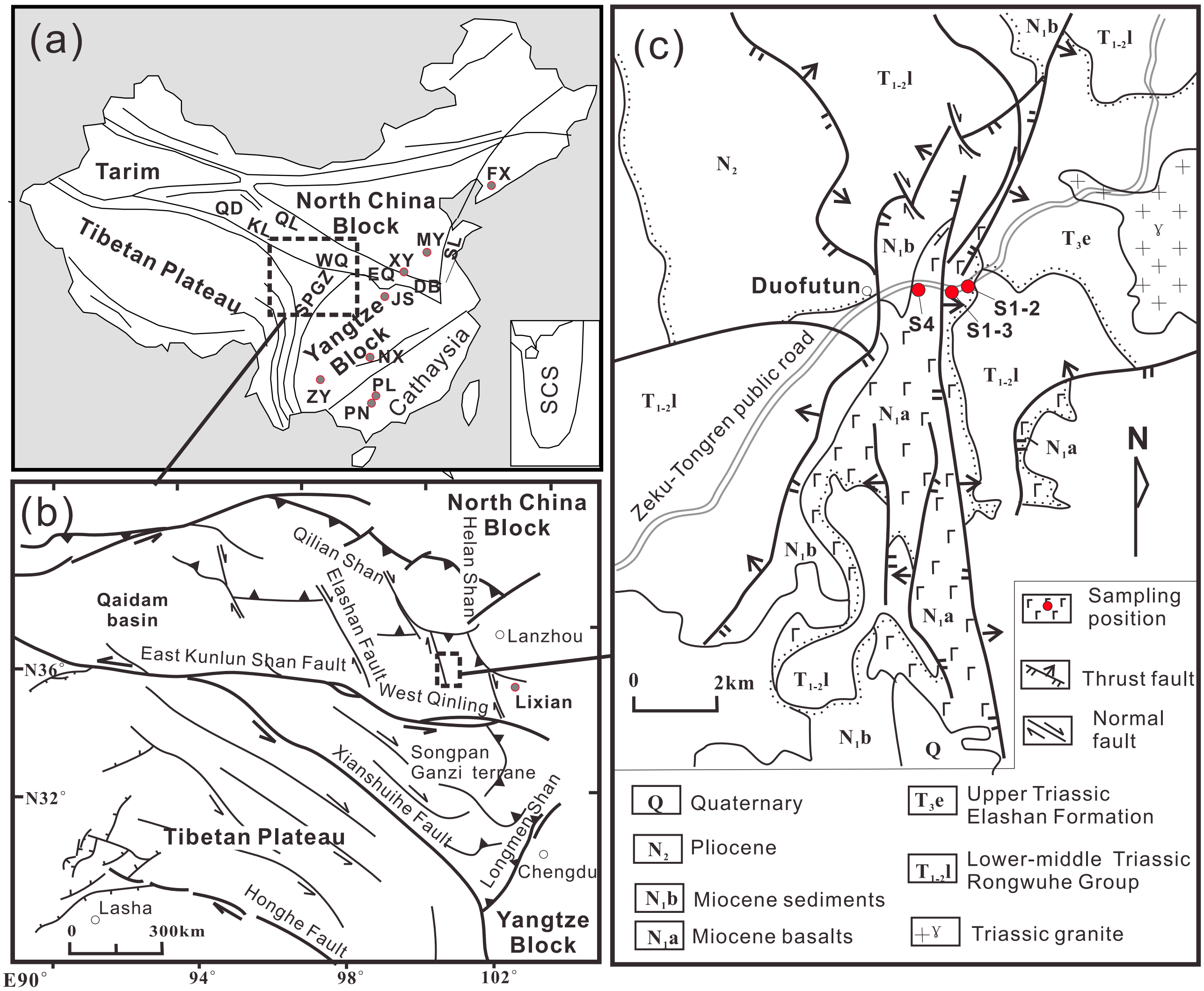

Figure 1. (a, b) Subdivision of the major tectonic units in China and (c) geological sketch map showing sampling localities (modified after *Guo et al.* [2007]). The dashed boxes in Figures 1a and 1b represent the local enlarged areas in Figures 1b and 1c, respectively. WQ, west Qinling terrane; SPGZ, Songpan-Ganzi terrane; EQ, east Qinling belt; DB, Dabie belt; SL, Sulu belt; QD, Qaidam; QL, Qilian Shan belt; KL, Kunlun Shan belt; SCS, South China Sea. The north China block: XY, Xinyang; MY, Mengyin; FX, Fuxian. The Yangtze block: JS, Jingshan; NX, Ningxiang; ZY, Zhenyuan. The Cathaysia block: PL, Pingle; PN, Pingnan.

where outcrops are mostly Phanerozoic, the U-Pb and Hf isotope data for zircons separated from three basalts in the Duofutun area (Figure 1c) of Qinghai Province are reported here. The data show that basaltic magmatism occurred at ~14 Ma in west Qinling region and that these magmas captured material from a highly evolved but unexposed Neoarchean (i.e., 2.7–2.5 Ga) basement. The zircon data allow us to interpret the timing and nature of tectonic events in the west Qinling orogenic terrane and thus to constrain its tectonic relationships to surrounding crustal blocks.

2. Geological Setting and Sampling

[4] The geologic framework of the eastern Qinling orogen was built up through the interplay of three blocks, the north China block (which includes the north Qinling), the south Qinling microcontinent, and the south China block (Figure 1a), separated by the Shangdan and Mianlue sutures [*Meng and Zhang*, 2000; *Ratschbacher et al.*, 2003]. The Shangdan suture resulted from the middle Paleozoic collision of the north China block and south Qinling, and the Mianlue suture resulted from the Late Triassic collision of the south Qinling and south China blocks. The present upper crust of the eastern Qinling orogen is dominated by thrust-fold systems. North Qinling displays thick-skinned deformation with involvement of the deep basement rocks, while south Qinling is characterized by thin-skinned thrusts and folds detached from the underlying rocks of lower Sinian ages [*Meng and Zhang*, 2000].

[5] The eastern Qinling orogen experienced a prolonged continental divergence and subsequent convergence between

the blocks. From late Neoproterozoic to early Paleozoic time, the south Qinling microcontinent formed the northern margin of the south China block, and the future north Qinling occupied the southern margin of the north China block, separated from the south Qinling-south China block by a proto-Tethyan Qinling Ocean. The north Qinling region evolved into an active convergent margin when the proto-Tethyan Qinling Ocean basin was subducted northward during the Ordovician. Collision between the south Qinling microcontinent and the north Qinling convergent belt took place in the middle Paleozoic along the Shangdan suture [*Enkin et al.*, 1992; *Yin and Nie*, 1996; *Hacker et al.*, 2004]. Synchronous with the collision, rifting occurred at the southern boundary of south Qinling, followed by the opening of the Paleo-Tethyan Qinling Ocean during the late Paleozoic, resulting in the splitting of the south China block from the south Qinling microcontinent. Collision of the south Qinling microcontinent and the south China block occurred in the Late Triassic along the Mianlue suture. The Late Triassic collisional event caused extensive fold-and-thrust deformation, was accompanied by intrusion of granitoid igneous rocks throughout the Qinling orogenic belt [*Zhang et al.*, 1997], and led to the final amalgamation of the north and south China blocks [*Zhai et al.*, 1998; *Sun et al.*, 2002].

[6] The north and south Qinling together make up the east Qinling block. The west Qinling belt is the westward extension of east Qinling and is bounded by the north China block to the north, the Qilian and Qaidam terranes to the west [*Zhou and Graham*, 1996], and the Songpan-Ganzi terranes to the south [*Weislogel et al.*, 2006] (Figure 1b). Basaltic rocks are distributed along WNW-trending faults [*Feng et al.*, 2003; *Fan et al.*, 2007]. They were originally regarded as the products of basaltic magmatism during the late Triassic-early Cretaceous (112 Ma, $^{40}Ar/^{39}Ar$ method [*Feng et al.*, 2003]) or Tertiary, as inferred from geological relationships by *Guo et al.* [2007].

[7] The samples studied here (S1-2, S1-3, and S4) were collected from the Duofutun area of Qinghai Province (Figure 1c). The basalts are mainly porphyritic with phenocrysts of olivine (2.0–2.5 mm across), pyroxene (2.5–3.5 mm across), or plagioclase (3–4 mm long) set in a groundmass of fine-grained plagioclase (0.2–0.5 mm long), clinopyroxene (0.3–0.8 mm across), and opaque minerals. Interstitial glass is common. All pyroxene and olivine have been replaced by chlorite. Sample S1-2 contains granulitic xenoliths consisting of granoblastic pyroxene (replaced by chlorite) and plagioclase (Figure 2a). Plagioclase phenocrysts are abundant in S1-3 (Figure 2b) but are few in S4 (Figure 2c).

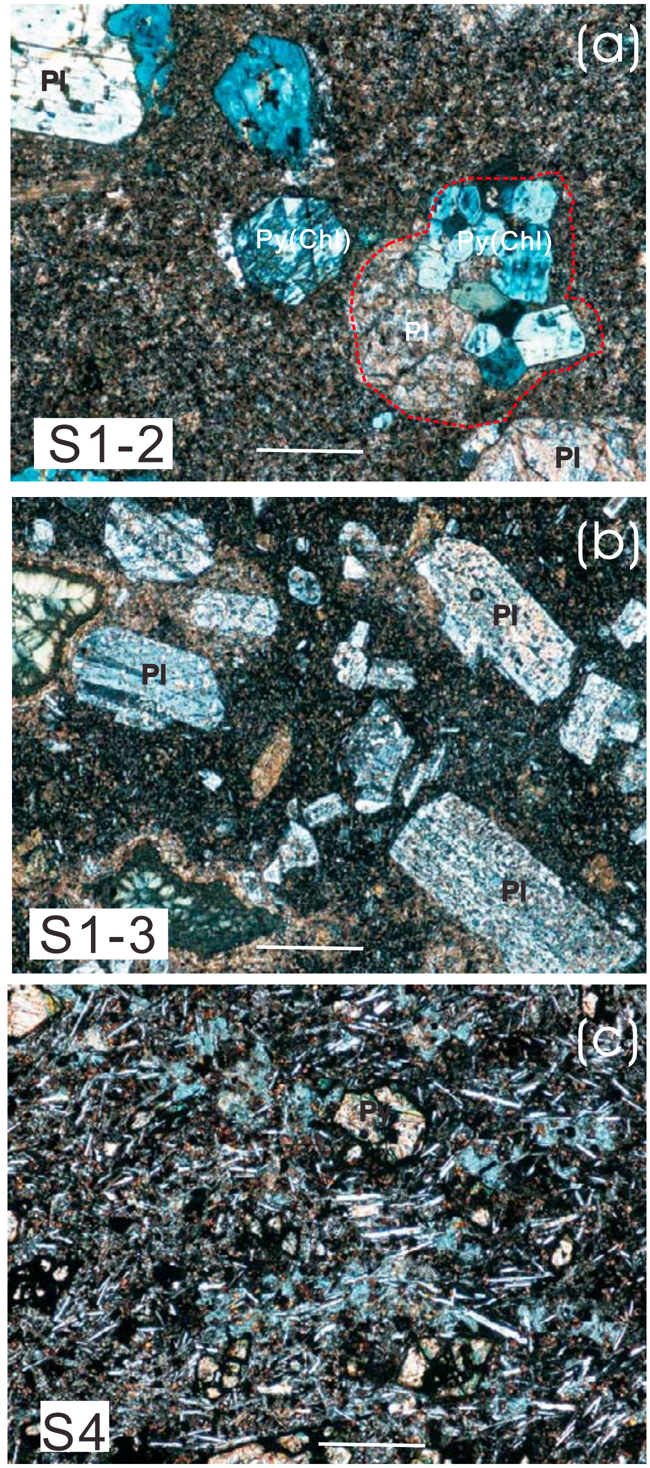

Figure 2. Photomicrographs of representative basalts from west Qinling. All have porphyritic microstructures: (a) sample S1-2, (b) sample S1-3, and (c) sample S4. (a) Sample S1-2 shows a granulite xenolith (circled). Plagioclase phenocrysts are abundant in S1-3 (Figure 2b) while scarce in S4 (Figure 2c). Pl, plagioclase; Py, pyroxene (fresh); Py (Chl), pyroxene replaced by chlorite. Scale bars = 2 mm.

3. Analytical Methods

[8] All analyses were carried out in the Australian Research Council National Key Centre for Geochemical Evolution and Metallogeny of Continents (GEMOC) at Macquarie University, New South Wales. Backscattered electron and cathodoluminescence (BSE/CL) images of each zircon (Figure 3) were taken using a Cameca SX-50 electron microprobe with a CL detector mounted, operating at 15 kV

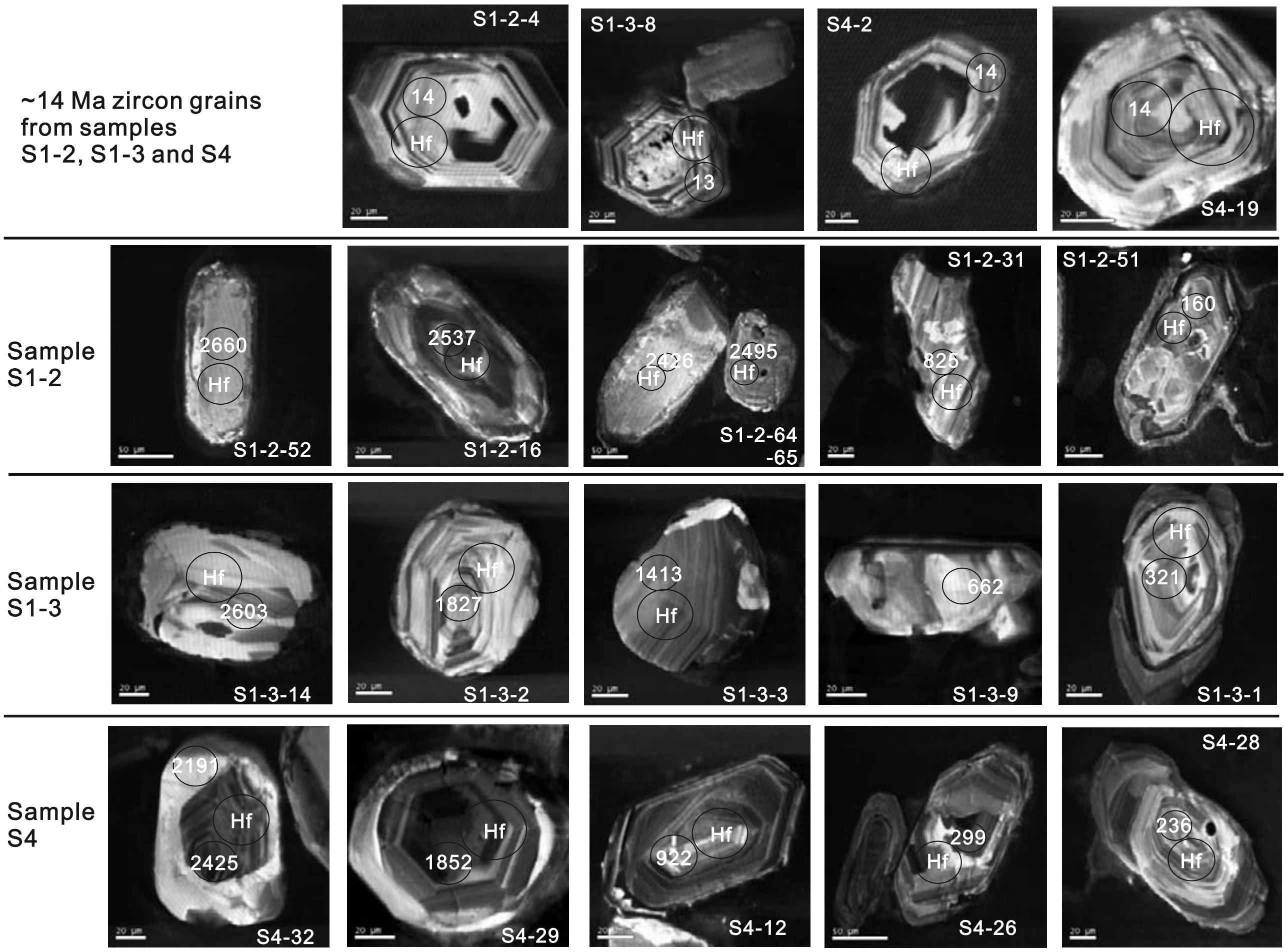

Figure 3. Representative CL images of zircon morphology and internal structure. The circles show positions for LAM-ICPMS and LAM-MC-ICPMS analyses (Table 1).

and 20 nA. These images have been used to recognize different types and stages of zircon growth, to distinguish igneous from recrystallized or metamorphic zircons, and to select the positions for laser ablation microbe inductively coupled plasma-mass spectrometry (LAM-ICPMS) U-Pb age and LAM multicollector ICPMS (LAM-MC-ICPMS) Hf isotope analyses.

3.1. U-Pb Dating

[9] In situ U-Pb isotope analyses of zircons (Table 1) were carried out using techniques described by *Belousova et al.* [2001] and *Jackson et al.* [2004]. Grain mounts containing the samples and GEMOC GJ1 zircon standard [*Belousova et al.*, 2001; *Jackson et al.*, 2004; *Griffin et al.*, 2008] were cleaned in 2 N nitric acid for ~1 h prior to analysis. LAM-ICPMS analyses were performed using a New Wave 213 nm UV LAM coupled with an Agilent 7500s ICPMS. ICPMS operating conditions and data acquisition parameters are given by *Belousova et al.* [2001]. Samples and standard were ablated in He gas to minimize deposition of ablation products around ablation sites and to improve sample transport efficiency; this also gives more stable signals and more reproducible Pb/U fractionation than ablation with Ar gas. To minimize dynamic U/Pb fractionation as the laser beam penetrates into the sample [*Hirata and Nesbitt*, 1995], analyses were performed with the laser focused above the sample (typically ~200 μm). Identical laser operating conditions were rigorously maintained throughout each run of 20 analyses to ensure constant U/Pb fractionation. Ablation pit diameters are generally about 40 μm.

[10] Samples were analyzed in "runs" of 20 analyses comprising 12 analyses of unknowns bracketed by four analyses of the GEMOC GJ1 zircon standard, a gem-quality zircon that contains ~260 ppm U; multiple thermal ionization mass spectroscopy (TIMS) analyses show the standard to be 608.5 ± 0.4 Ma old ($^{207}Pb/^{206}Pb$ age) and slightly discordant [*Belousova et al.*, 2001; *Jackson et al.*, 2004; *Griffin et al.*, 2008]. Each analysis was ~180 s, gas background measurements being taken over the first ~60 s, before initiation of ablation. Data were acquired on five masses (206–208, 232, 238) with short dwell times to provide quasi-simultaneous measurement of the five masses and optimum precision. Time-resolved signals (i.e., signals as a function of time, which is a proxy for ablation depth)

Table 1. U-Pb Data for Zircons From the Western Qinling Basaltic Rocks[a]

Sample Grains	Size (μm)	Shape: External	Shape: Core	Zoning	$^{207}Pb/^{206}Pb$	1s	$^{207}Pb/^{235}U$	1s	$^{206}Pb/^{238}U$	1s	$^{208}Pb/^{232}Th$	1s	Th/U	$^{207}Pb/^{206}Pb$ (Ma)	1s	$^{207}Pb/^{235}U$ (Ma)	1s	$^{206}Pb/^{238}U$ (Ma)	1s	$^{208}Pb/^{232}Th$ (Ma)	1s
Sample S1-2 (35°N 16'39.7" and 101°E 56'00.4")																					
S1-2-1c			E	L	0.06830	0.00086	1.35743	0.01879	0.14415	0.00172	0.04559	0.00047	0.55	878	26	871	8.1	868	10	901	9.2
S1-2-1r	70 × 145	S		N	0.04993	0.00208	0.01577	0.00065	0.00229	0.00003	0.00077	0.00002	0.56	192	94	15.9	0.7	14.8	0.2	15.6	0.3
S1-2-4	80 × 115	E		O	0.04644	0.00110	0.01398	0.00034	0.00218	0.00003	0.00072	0.00001	0.46	20.6	55	14.1	0.3	14.1	0.2	14.5	0.2
S1-2-7	100 × 145	I		I	0.17013	0.00334	0.06530	0.00127	0.00278	0.00004	0.00180	0.00002	0.81	2559	32	64	1.2	17.9	0.2	36	0.5
S1-2-11	85 × 125	I		L	0.06950	0.00080	1.40282	0.01817	0.14639	0.00174	0.04542	0.00045	1.04	914	24	890	7.7	881	10	898	8.6
S1-2-16	60 × 115	S	S	N	0.16787	0.00186	10.99617	0.13780	0.47509	0.00564	0.14090	0.00140	0.20	2537	18	2523	12	2506	25	2664	25
S1-2-18	65 × 95	E		O	0.06649	0.00077	1.11968	0.01447	0.12213	0.00145	0.03843	0.00038	0.47	822	24	763	6.9	743	8.3	762	7.5
S1-2-26	65 × 70	I		N	0.16364	0.00186	10.81536	0.13815	0.47934	0.00571	0.14407	0.00147	0.40	2494	19	2507	12	2524	25	2720	26
S1-2-29	80 × 155	S		I	0.06652	0.00075	1.23591	0.01575	0.13474	0.00160	0.04202	0.00042	0.53	823	23	817	7.2	815	9.1	832	8.1
S1-2-31	55 × 125	I		L	0.06671	0.00081	1.25594	0.01692	0.13655	0.00163	0.03772	0.00039	0.58	829	25	826	7.6	825	9.3	748	7.6
S1-2-32	60 × 110	S	E	N	0.07796	0.00092	1.61586	0.02135	0.15033	0.00179	0.04850	0.00048	1.11	1146	23	976	8.3	903	10	957	9.4
S1-2-40	55 × 110	E		O	0.05630	0.00203	0.01732	0.00062	0.00223	0.00003	0.00082	0.00002	0.58	463	78	17.4	0.6	14.4	0.2	16.6	0.3
S1-2-41	60 × 100	S		O	0.04787	0.00148	0.01460	0.00045	0.00221	0.00003	0.00073	0.00001	0.77	91.8	73	14.7	0.5	14.2	0.2	14.8	0.2
S1-2-44	70 × 120	I	E	O	0.07862	0.00096	1.63454	0.02208	0.15079	0.00180	0.04954	0.00050	1.69	1163	24	984	8.5	905	10	977	10
S1-2-45c			I	N	0.05189	0.00102	0.01955	0.00040	0.00273	0.00003	0.00219	0.00005	0.04	281	44	19.7	0.4	17.6	0.2	44.3	1.0
S1-2-45r	75 × 180	E		O	0.04797	0.00088	0.01714	0.00033	0.00259	0.00003	0.00084	0.00002	0.07	96.9	44	17.3	0.3	16.7	0.2	16.9	0.4
S1-2-51	110 × 210	S	S	I	0.04924	0.00082	0.17082	0.00299	0.02516	0.00031	0.00808	0.00010	0.49	159	39	160	2.6	160	1.9	163	1.9
S1-2-52	65 × 155	S	I	N	0.18077	0.00210	12.72283	0.16604	0.51047	0.00611	0.13777	0.00141	0.86	2660	19	2659	12	2659	26	2609	25
S1-2-53	80 × 195	E	I	O	0.05605	0.00240	0.01636	0.00069	0.00212	0.00003	0.00074	0.00002	0.37	454	93	16.5	0.7	13.6	0.2	14.9	0.4
S1-2-64	100 × 195	S		N	0.15719	0.00183	9.56751	0.12489	0.44146	0.00528	0.12219	0.00125	0.71	2426	20	2394	12	2357	24	2330	23
S1-2-65	90 × 110	S		N	0.16382	0.00315	10.07378	0.19760	0.44601	0.00613	0.19373	0.00522	0.15	2495	32	2442	18	2378	27	3579	88
S1-2-67	90 × 165	I	E	O	0.06774	0.00086	1.29475	0.01793	0.13863	0.00165	0.04324	0.00045	0.61	861	26	843	7.9	837	9.4	856	8.6
S1-2-68	110 × 180	E		O	0.06226	0.00235	0.02019	0.00075	0.00235	0.00003	0.00092	0.00002	0.63	683	78	20.3	0.8	15.1	0.2	18.5	0.4
Sample S1-3 (35°N 13'31.011" and 101°E 50'05.8")																					
S1-3-1	55 × 95	S		O	0.05334	0.00101	0.37497	0.00731	0.05099	0.00063	0.01642	0.00020	0.76	343	42	323	5.4	321	3.9	329	4.0
S1-3-2	75 × 80	R		O	0.11165	0.00139	5.01841	0.06901	0.32599	0.00393	0.09475	0.00102	0.65	1827	22	1822	12	1819	19	1830	19
S1-3-3	70 × 80	I		O	0.08942	0.00121	2.89838	0.04248	0.23507	0.00285	0.07076	0.00082	0.43	1413	26	1382	11	1361	15	1382	16
S1-3-8	75 × 90	E	I (N)	O	0.05545	0.00077	0.01580	0.00024	0.00207	0.00002	0.00073	0.00001	0.47	430	30	15.9	0.2	13.3	0.2	14.7	0.2
S1-3-9	50 × 100	I		N	0.06462	0.00079	0.96348	0.01311	0.10813	0.00130	0.02616	0.00027	1.12	762	26	685	6.8	662	7.6	522	5.4
S1-3-10	50 × 95	S		N	0.06681	0.00095	0.36174	0.00553	0.03927	0.00048	0.01511	0.00017	0.53	832	29	314	4.1	248	3.0	303	3.4
S1-3-14	75 × 90	I		L	0.17467	0.00221	11.22252	0.15647	0.46598	0.00566	0.13524	0.00148	0.97	2603	21	2542	13	2466	25	2564	26
Sample S4 (35°N 12'20.9" and 101°E 48'37.0")																					
S4-2	65 × 90	E	I (N)	O	0.05703	0.00107	0.01655	0.00032	0.00211	0.00003	0.00070	0.00001	1.92	492	41	16.7	0.3	13.6	0.2	14.2	0.2
S4-8	70 × 90	I		O	0.13443	0.00171	0.73570	0.01029	0.03969	0.00048	0.03628	0.00039	0.35	2157	22	560	6.0	251	3.0	720	7.7
S4-9	60 × 100	E		O	0.06688	0.00154	0.01979	0.00046	0.00215	0.00003	0.00087	0.00001	0.63	834	47	19.9	0.5	13.8	0.2	17.6	0.3
S4-10	70 × 100	S		O	0.06338	0.00095	0.60006	0.00960	0.06867	0.00084	0.02596	0.00031	0.37	721	31	477	6.1	428	5.1	518	6.1
S4-12	60 × 105	E		O	0.06931	0.00089	1.46996	0.02075	0.15382	0.00186	0.05321	0.00061	0.18	908	26	918	8.5	922	10	1048	12
S4-14	70 × 95	I		N	0.09367	0.00193	1.86083	0.03911	0.14408	0.00189	0.04443	0.00059	1.23	1501	39	1067	14	868	11	879	11
S4-15	55 × 95	S		O	0.07573	0.00122	0.40486	0.00690	0.03877	0.00048	0.01824	0.00023	1.41	1088	32	345	5.0	245	3.0	365	4.5
S4-16	55 × 80	S	E	O	0.08397	0.00133	0.44789	0.00749	0.03869	0.00048	0.02166	0.00027	0.33	1292	31	376	5.3	245	3.0	433	5.4
S4-17	65 × 100	S	S	O	0.15375	0.00253	0.94118	0.01607	0.04440	0.00056	0.03581	0.00045	0.48	2388	28	674	8.4	280	3.5	711	8.7
S4-19	65 × 85	E		O	0.04654	0.00129	0.01345	0.00038	0.00210	0.00003	0.00075	0.00001	0.53	25.7	64	13.6	0.4	13.5	0.2	15.1	0.2
S4-20	60 × 75	E	E	O	0.06894	0.00120	0.36309	0.00660	0.03820	0.00048	0.01621	0.00021	0.43	897	36	315	4.9	242	3.0	325	4.2
S4-26	80 × 175	E		O	0.05235	0.00110	0.34297	0.00738	0.04751	0.00060	0.01585	0.00023	0.45	301	47	299	5.6	299	3.7	318	4.6
S4-27	55 × 195	S	E	O	0.05818	0.00114	0.30521	0.00618	0.03805	0.00048	0.01326	0.00019	0.37	536	43	271	4.8	241	3.0	266	3.9
S4-28	70 × 110	S		O	0.05128	0.00113	0.26390	0.00595	0.03732	0.00048	0.01242	0.00017	0.68	254	50	238	4.8	236	3.0	250	3.4
S4-29	80 × 85	S	E	O	0.11321	0.00148	5.19306	0.07465	0.33269	0.00404	0.10040	0.00118	0.20	1852	23	1852	12	1851	20	1934	22
S4-31	95 × 145	E	S	N	0.04748	0.00190	0.01424	0.00056	0.00218	0.00003	0.00079	0.00002	0.37	72.6	93	14.4	0.6	14.0	0.2	15.9	0.4
S4-32c		I		N	0.15713	0.00210	8.80205	0.12907	0.40628	0.00496	0.11823	0.00136	1.15	2425	23	2318	13	2198	23	2259	25
S4-32r	70 × 95		I	O	0.13713	0.00184	7.17335	0.10516	0.37938	0.00463	0.10561	0.00120	1.67	2191	23	2133	13	2073	22	2029	22
S4-41	75 × 110	S	S	O	0.05078	0.00138	0.25001	0.00686	0.03571	0.00047	0.01245	0.00021	0.49	231	62	227	5.6	226	3.0	250	4.2
S442	90 × 130	I		N	0.10564	0.00145	4.21795	0.06318	0.28957	0.00354	0.08691	0.00103	0.50	1726	25	1678	12	1639	18	1684	19

[a]R, rounded; I, irregular; S, subhedral; E, euhedral; O, oscillatory; L, lamellar; N, no internal structure.

allow isotopic heterogeneity within the ablation volume to be clearly identified (i.e., zones of Pb loss or common Pb related to fractures or areas of radiation damage; also inclusions, inherited cores, etc.).

[11] Raw data were processed using the GLITTER online data reduction program [*Griffin et al.*, 2008/] (see http://www.es.mq.edu.au/GEMOC/). The ratios $^{207}Pb/^{206}Pb$, $^{208}Pb/^{232}Th$, $^{206}Pb/^{238}U$, and $^{207}Pb/^{235}U$ ($^{235}U = ^{238}U/137.88$) were calculated for each mass sweep, and the time-resolved ratios for each analysis were then carefully examined. Optimal signal intervals for the background and ablation data were selected for each sample and were automatically matched with identical time intervals for the standard zircon analyses, thus correcting for the effects of ablation-/transport-related U-Pb fractionation and mass bias of the mass spectrometer. Net background-corrected count rates for each isotope were used for calculation of sample ages. Furthermore, U and Th contents and thus Th/U ratios were estimated by direct comparison of integrated count rates with those on the GJ1 standard [*Belousova et al.*, 2001; *Jackson et al.*, 2004].

[12] The ^{204}Pb isotope cannot be precisely measured with this technique, because of a combination of low signal and interference from small amounts of ^{204}Hg in the Ar gas supply. Common Pb contents were therefore evaluated by using the method described by *Andersen* [2002]; in nearly all cases, Pb contents were below the level of detection (<0.2%), and no correction was applied. The precision and accuracy obtained with this technique have been illustrated by comparison with TIMS data for some well-characterized zircons [*Jackson et al.*, 2004]. Concordia ages were determined using Isoplot 2.32 [*Ludwig*, 2000].

3.2. Hf Isotope Analysis

[13] Hf isotope analyses (Table 2) were carried out in situ with a Merchantek EO LUV 213 nm laser-ablation microprobe attached to a Nu plasma MC-ICPMS on the same grains, using techniques described in detail by *Griffin et al.* [2000, 2002]. Interference of ^{176}Lu on ^{176}Hf has been corrected by measuring the intensity of the interference-free ^{175}Lu isotope and using the recommended $^{176}Lu/^{175}Lu$ = 0.02669 [*Debievre and Taylor*, 1993] to calculate $^{176}Lu/^{177}Hf$. Similarly, the interference of ^{176}Yb on ^{176}Hf has been corrected by measuring the interference-free ^{172}Yb isotope and using $^{176}Yb/^{172}Yb$ to calculate $^{176}Yb/^{177}Hf$. The appropriate value of $^{176}Yb/^{172}Yb$ was determined by spiking the JMC475 Hf standard with Yb and determining the value of $^{176}Yb/^{172}Yb$ (0.58669) required to yield the value of $^{176}Hf/^{177}Hf$ obtained on the pure Hf solution. Most LAM analyses were carried out in Ar carrier gas with a beam diameter of ~80 μm, a 10 Hz repetition time, and energies of 0.6–1.3 mJ/pulse. Typical ablation times were 80–120 s, resulting in pits 40–60 μm deep. For the calculation of ε_{Hf} values we have adopted the chondritic values of *Blichert-Toft and Albarede* [1998]. The precision and accuracy of the analysis and the calculation of model ages are described in detail by *Griffin et al.* [2000, 2002]. Typical precision on $^{176}Hf/^{177}Hf$ is ± 0.00003 (2σ) or approximately ±1 ε_{Hf}. The calculation of model ages is based on the depleted-mantle source and using 1.865×10^{-11} for the ^{176}Lu decay constant. Table 2 reports both T_{DM} model ages, calculated using the measured Lu/Hf of zircon, and T_{crust} model ages, which assume that the protolith from which the host magma of a given zircon was derived from the depleted-mantle source, and has the $^{176}Lu/^{177}Hf$ of the average continental crust (= 0.015 [*Griffin et al.*, 2000]).

4. Results

4.1. Zircon Morphology and Internal Structure

[14] All zircons were imaged by BSE/CL as described above, and 50 grains from each of the three studied samples were selected for U-Pb age analysis. The external forms of the grains have been classified as mainly subhedral (~50%), with ~30% irregular, ~20% euhedral, and one rounded grain (S1-3–2; see Table 1). Internal zoning structures of cores and rim areas of the zircons have been classified as mainly oscillatorily zoned or structureless, with less common lamellar and irregular structure. The images reveal the presence of distinct cores, recognized by different zoning patterns, in ~40% of the grains. Most cores are euhedral or subhedral and are surrounded by unzoned rims; however, some cores (i.e., grains S1-3–8 and S4–2) are irregular and structureless and are surrounded by euhedral forms with oscillatorily zoned structure (Figure 3).

4.2. U-Pb Dating

[15] Zircons from sample S1-2 are transparent, light yellow to colorless, and mainly subhedral (~50%), ~25% being euhedral and ~25% irregular in form (55–210 μm). Their length-to-width ratios are 1.0–2.4 with a mean of 2.1. Nearly half of the grains have oscillatorily zoned cores, and ~35% show no internal structure. Three grains are lamellar or irregular. The oldest concordant age of 2660 ± 19 Ma is given by S1-2–52 (Figure 4a), a subhedral grain with uniform internal structure and Th/U = 0.86. Four concordant to near-concordant grains (S1-2–16, −26, −64, and −65) give old $^{207}Pb/^{206}Pb$ ages (i.e., ~2.5–2.4 Ga). They also show no internal structure and have Th/U = 0.20–0.71. Other concordant grains give $^{206}Pb/^{238}Pb$ ages that are Neoproterozoic (820–880 Ma, n = 5; Figure 4b), late Mesozoic (160 Ma, S1-2–51; Figure 4c), and Neogene (13.6–17.9 Ma, n = 9). Most grains with Neoproterozoic ages show oscillatory or lamellar internal structures and have high Th/U ratios (up to 1.69). Two grains (S1-2–1 and S1-2–45) were analyzed for core and rim; both rims give Neogene ages (14.8–16.7 Ma), while the cores are Neoproterozoic (868 ± 10 Ma for S1-2–1) or Neogene (17.6 ± 0.2 Ma for S1-2–45). Seven of the nine Neogene grains yield a lower intercept age of 14.2 ± 0.2 Ma (inset of Figure 4c). These Neogene grains are euhedral to subhedral in form and have oscillatory zoning.

[16] Zircons from sample S1-3 are colorless to light brown and transparent. They range from euhedral through subhedral and from irregular to round in form (50–100 μm), with length-to-width ratios of 1.1–2.0 (mean 1.5). Most grains have oscillatorily zoned cores, but some show no internal structure. One grain (S1-3–14) with lamellar internal structure gives a near-concordant age of 2603 ± 21 Ma (Figure 5). Other concordant or near-concordant grains give $^{207}Pb/^{206}Pb$ ages of 1827 ± 22 Ma (S1-3–2) and 1413 ± 26 Ma

Table 2. Lu-Hf Isotopes of Zircons From the Western Qinling Basaltic Rocks[a]

Analysis ID	Shape External	Shape Core	Zoning	$^{176}Hf/^{177}Hf$	1s	$^{176}Lu/^{177}Hf$	$^{176}Yb/^{177}Hf$	Age (Ma)	Hf_i	ε_{Hf}	1s	T_{DM} (Ga)	T_{crust} (Ga)
Sample S1-2													
S1-2-1c		E	L	0.282599	0.000011	0.001507	0.065173	868	0.282574	12.2	0.4	0.9	1.0
S1-2-1r	S		N	0.282784	0.000011	0.000816	0.026085	14.8	0.282784	0.7	0.4	0.7	1.1
S1-2-4	E		O	0.282813	0.000008	0.000968	0.040987	14.1	0.282813	1.7	0.3	0.6	1.0
S1-2-7	I		I	0.282792	0.000007	0.000901	0.041337	17.9	0.282792	1.1	0.2	0.7	1.0
S1-2-11	I		L	0.282506	0.000014	0.001716	0.074823	881	0.282478	9.0	0.5	1.1	1.2
S1-2-16	S	S	N	0.281305	0.000014	0.001071	0.031869	2537	0.281253	3.2	0.5	2.7	2.9
S1-2-26	I		N	0.281360	0.000006	0.000236	0.011355	2494	0.281349	5.6	0.2	2.6	2.7
S1-2-29	S		I	0.282140	0.000010	0.002836	0.144183	815	0.282097	−5.9	0.3	1.6	2.1
S1-2-31	I		L	0.282538	0.000012	0.001637	0.063578	825	0.282513	9.1	0.4	1.0	1.2
S1-2-32	S	E	N	0.281976	0.000013	0.000740	0.032001	1146	0.281960	−3.4	0.5	1.8	2.2
S1-2-40	E		O	0.282751	0.000015	0.001703	0.046744	14.4	0.282751	−0.4	0.5	0.7	1.1
S1-2-41	E		O	0.282663	0.000019	0.001601	0.043340	14.2	0.282663	−3.6	0.7	0.8	1.3
S1-2-44	I	E	O	0.282488	0.000012	0.001998	0.105314	1163	0.282444	14.2	0.4	1.1	1.1
S1-2-45r	E		O	0.282770	0.000008	0.001165	0.043723	17.6	0.282770	0.3	0.3	0.7	1.1
S1-2-51	S	S	I	0.282601	0.000013	0.000732	0.036744	160	0.282599	−2.6	0.5	0.9	1.4
S1-2-52	S	I	N	0.281399	0.000019	0.001483	0.063700	2660	0.281324	8.5	0.7	2.6	2.6
S1-2-53	S	I	O	0.282781	0.000007	0.000532	0.022096	13.6	0.282781	0.6	0.3	0.7	1.1
S1-2-64	S		N	0.281446	0.000009	0.000766	0.029655	2426	0.281411	6.2	0.3	2.5	2.6
S1-2-65	S		N	0.281284	0.000014	0.000240	0.011922	2495	0.281273	2.9	0.5	2.7	2.8
S1-2-67c	I	E	O	0.282520	0.000022	0.001891	0.074982	837	0.282490	8.5	0.8	1.1	1.2
S1-2-67r				0.282523	0.000011	0.001408	0.065813	837	0.282501	8.9	0.4	1.0	1.2
S1-2-68	E		O	0.282809	0.000009	0.000748	0.026738	15.1	0.282809	1.6	0.3	0.6	1.0
Sample S1-3													
S1-3-1	S		O	0.282208	0.000016	0.002364	0.072545	321	0.282194	−13.4	0.6	1.5	2.2
S1-3-2	R		O	0.281849	0.000014	0.001340	0.059650	1827	0.281803	6.4	0.5	2.0	2.1
S1-3-3	I		O	0.281985	0.000021	0.001585	0.048903	1413	0.281943	2.0	0.7	1.8	2.1
S1-3-8	E	I (N)	O	0.282885	0.000011	0.002401	0.081261	13.3	0.282884	4.3	0.4	0.5	0.8
S1-3-10	S		N	0.282464	0.000013	0.001567	0.053701	248	0.282457	−5.7	0.5	1.1	1.6
S1-3-14	I		L	0.281087	0.000009	0.000639	0.028270	2603	0.281055	−2.3	0.3	3.0	3.3
Sample S4													
S4-2	E	I (N)	O	0.282775	0.000010	0.001268	0.039631	13.6	0.282775	0.4	0.3	0.7	1.1
S4-8	I		O	0.282476	0.000009	0.000658	0.032551	251	0.282473	−5.1	0.3	1.1	1.6
S4-9	E		O	0.282782	0.000012	0.001105	0.057638	13.8	0.282782	0.6	0.4	0.7	1.1
S4-10	S		O	0.282383	0.000010	0.001244	0.045441	428	0.282373	−4.7	0.4	1.2	1.7
S4-12	E		O	0.282080	0.000033	0.005945	0.204242	922	0.281977	−7.8	1.2	1.9	2.3
S4-14	I		N	0.281513	0.000013	0.000393	0.016390	868	0.281507	−25.6	0.5	2.4	3.4
S4-15	S		O	0.282391	0.000016	0.001406	0.044487	245	0.282385	−8.3	0.6	1.2	1.8
S4-17	S	S	O	0.282420	0.000015	0.000161	0.007467	280	0.282419	−6.3	0.5	1.2	1.7
S4-19	S	E	O	0.282763	0.000016	0.000902	0.025004	13.5	0.282763	0.0	0.6	0.7	1.1
S4-20	E	E	O	0.282473	0.000012	0.001150	0.052122	242	0.282468	−5.5	0.4	1.1	1.6
S4-26	E		O	0.282490	0.000015	0.001134	0.071166	299	0.282484	−3.6	0.5	1.1	1.6
S4-27	S	E	O	0.282552	0.000016	0.001283	0.045384	241	0.282546	−2.7	0.6	1.0	1.4
S4-28	S		O	0.282479	0.000010	0.000680	0.034351	236	0.282476	−5.3	0.3	1.1	1.6
S4-29	S	E	O	0.281423	0.000007	0.001752	0.082036	1852	0.281361	−8.7	0.2	2.6	3.1
S4-31	E	S	N	0.282790	0.000008	0.000800	0.032015	14.0	0.282790	0.9	0.3	0.7	1.0
S4-32c	I		N	0.281349	0.000012	0.001004	0.037393	2425	0.281303	2.4	0.4	2.7	2.8
S4-41	S	S	O	0.282498	0.000009	0.000902	0.041485	226	0.282494	−4.9	0.3	1.1	1.6
S4-42	I		N	0.281844	0.000013	0.001016	0.041498	1726	0.281811	4.4	0.5	2.0	2.1

[a]R, rounded; I, irregular; S, subhedral; E, euhedral; O, oscillatory; L, lamellar; N, no internal structure.

(S1-3–3) and $^{206}Pb/^{238}Pb$ ages of 662 ± 8 Ma (S1-3–9), 321 ± 4 Ma (S1-3–1), and 13.3 ± 0.2 Ma (S1-3–8).

[17] Zircons from sample S4 are transparent, light purple to colorless. They are mainly subhedral, with some euhedral and irregular in form; diameters range from 55 to 195 μm and length-to-width ratios from 1.1 to 3.5 (mean 1.4). All show oscillatory zoning except for four zircons that show no internal structure. The core and rim of grain S4 was analyzed and gave $^{207}Pb/^{206}Pb$ ages of 2425±23 Ma (mildly discordant) and 2191 ± 23 Ma (near-concordant; Figure 6a), respectively, suggesting the grain is at least older than 2200 Ma. Another concordant grain gave a $^{207}Pb/^{206}Pb$ age of 1852 ± 23 Ma (S4-29), and concordant $^{206}Pb/^{238}Pb$ ages are 922 ± 10 Ma (S4-12), 299 ± 4 Ma (S4-26), 226 ± 3 Ma (S4-41), and 13.5 ± 0.2 Ma (S4-19). Seven early Mesozoic grains with significant common Pb content yield an intercept age of 230 ± 3 Ma (Figure 6b). These grains are euhedral to subhedral in shape and have oscillatory zoning. Four Neogene grains with mostly euhedral external shapes yielded a lower intercept age of 13.8 ± 0.2 Ma (Figure 6c).

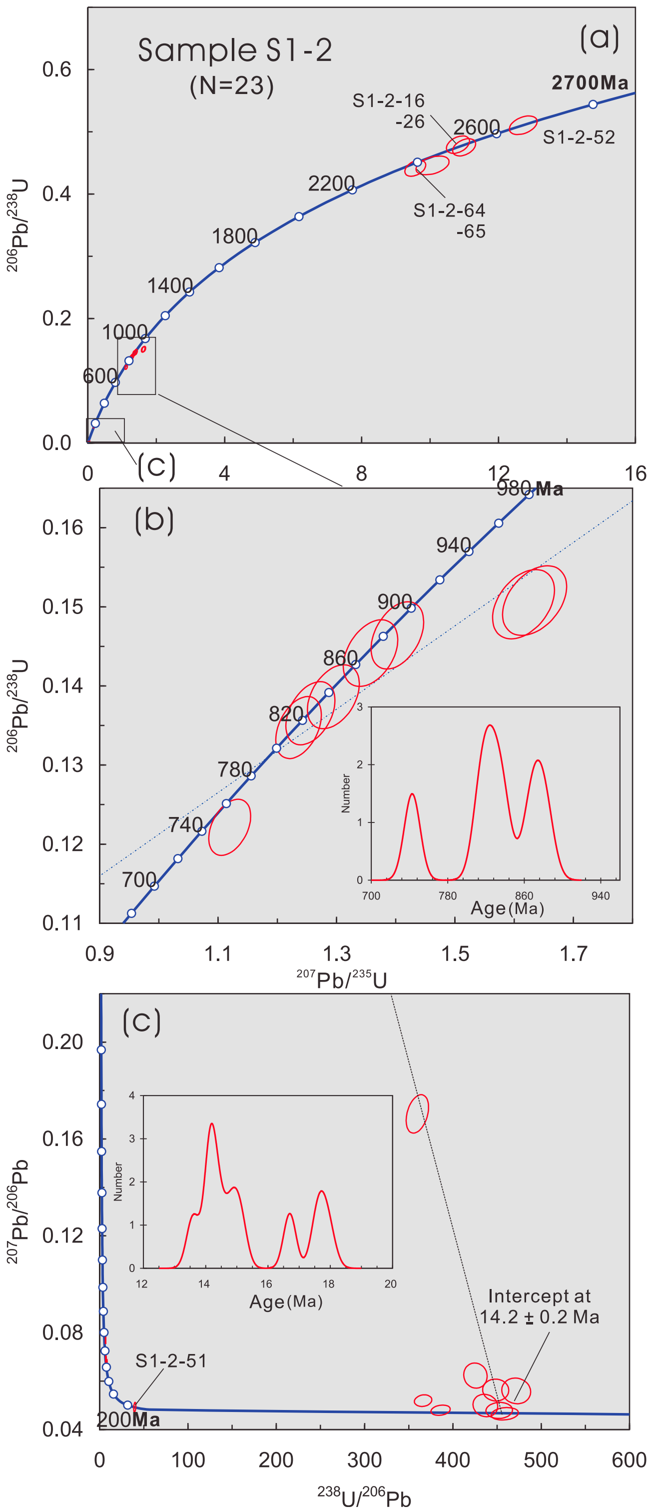

Figure 4. Concordia plots (a) of U-Pb results for zircons in sample S1-2. (b, c) The local enlarged areas from Figure 4a. Insets in Figures 4b and 4c represent probability density.

4.3. Hf Isotopes

[18] All Neoarchean to early Paleoproterozoic (i.e., 2.7–2.4 Ga) zircons (except S1-3–14) have positive ε_{Hf} (up to +8.5), with a narrow range of T_{DM} (2.5–2.7 Ga) and T_{crust} (2.6–2.9 Ga). Grain S1-3–14, with an age of 2603 Ma and lamellar internal structure, has negative ε_{Hf} (−2.3) and thus gives a slightly higher T_{DM} (3.0 Ga) and T_{crust} (3.3 Ga), suggesting that the generation of the host magma involved older (at least 3.0 Ga) crustal components (Figure 7).

[19] All late Paleoproterozoic zircons (1.7–1.85 Ga) except S4-29 and the single Mesoproterozoic (~1.4 Ga) grain also have positive ε_{Hf} (2.0–6.4) and have T_{DM} = 1.8–2.0 Ga and T_{crust} ≈ 2.1 Ga. Grain S4-29, which displays oscillatory zoning and a euhedral core, has negative ε_{Hf} (−8.7) and high T_{DM} (2.6 Ga) and T_{crust} (3.1 Ga). Most Neoproterozoic (0.8–1.1 Ga) zircons have positive ε_{Hf} (up to +14.2) and give similar T_{DM} (0.9–1.1 Ga) and T_{crust} (1.0–1.2 Ga), showing the addition of depleted-mantle material in Neoproterozoic time. The others have negative ε_{Hf} (i.e., down to −25.6 in S4-14) and have a wide range of T_{DM} (1.6–2.4 Ga) and T_{crust} (2.1–3.4 Ga). If these are igneous grains (i.e., Th/U = 0.2–1.2), their Hf isotope compositions reflect the assimilation of old crustal components. The components may be similar to the crustal rocks represented by grains S1-3–14 and S4-14, which lie on the evolution line for a 3.0 Ga source with ^{176}Lu/^{177}Hf = 0.013 similar to the average continental crust (Figure 7). The Paleozoic-Mesozoic zircons have negative ε_{Hf} and T_{DM} = 0.9–1.2 Ga and T_{crust} ≈1.4–1.8 Ga. The Neogene grains have near-zero ε_{Hf} (−3.6 to +4.3) and give T_{DM} = 0.6–0.8 Ga and T_{crust} ≈ 0.8–1.3 Ga.

5. Discussion

5.1. Neogene (~14 Ma) Magmatism in West Qinling

[20] Thirteen zircon grains among the 51 recovered from the studied samples are euhedral (Table 1 and Figure 3). The

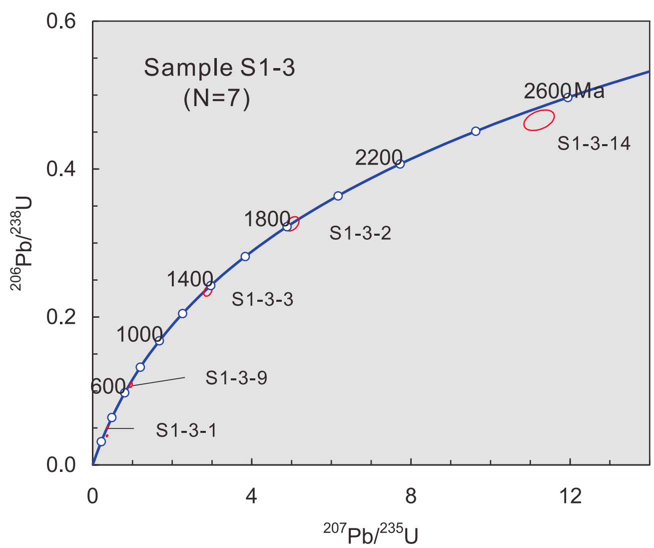

Figure 5. Concordia plots of U-Pb results for zircons in sample S1-3.

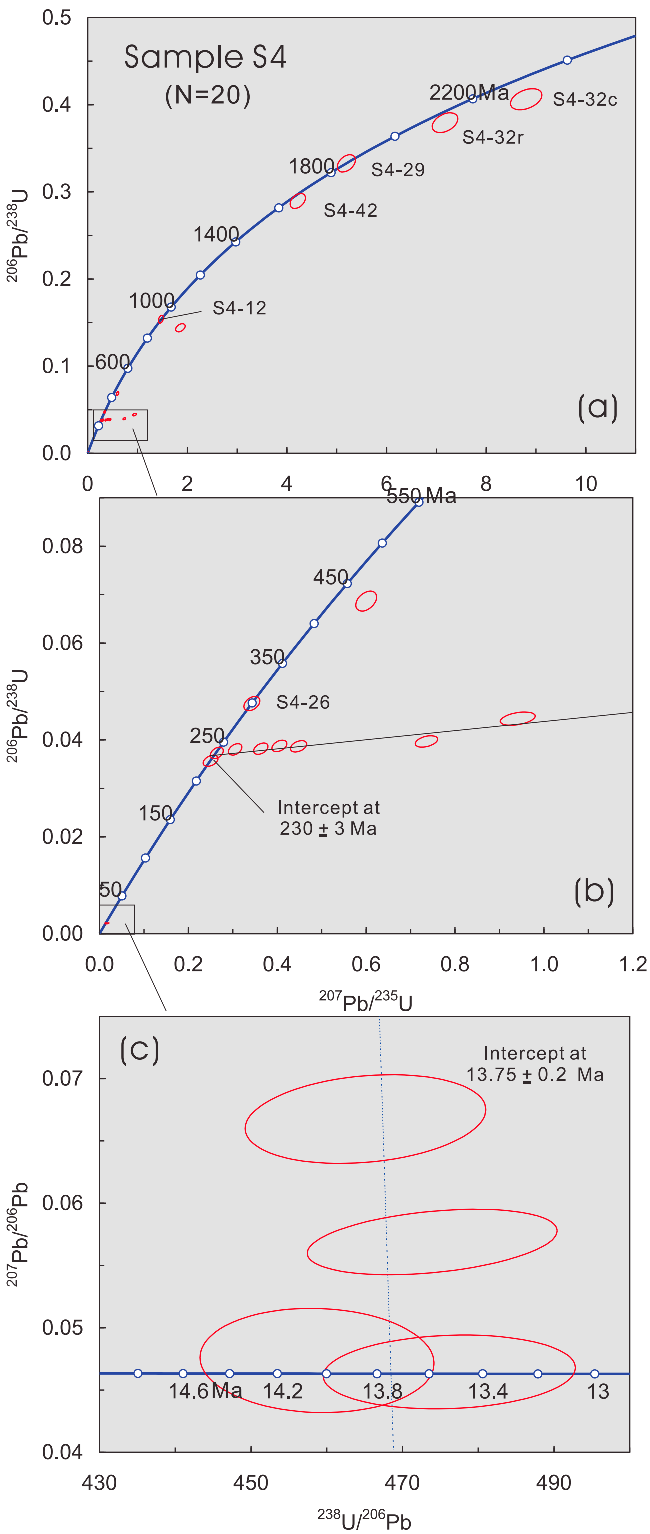

Figure 6. (a) Concordia plots of U-Pb results for zircons in sample S4. (b, c) The local enlarged areas from Figures 6a and 6b, respectively.

$^{206}Pb/^{238}U$ ages of these euhedral zircons, and the lower intercept ages of two samples (i.e., S1-2 and S4), are ~14 Ma, suggesting that the basaltic magmatism occurred in Neogene time, rather than late Mesozoic as suggested by the whole-rock $^{40}Ar/^{39}Ar$ age (112 Ma [*Feng et al.*, 2003]); the 14 Ma age is consistent with the geological relationships of the basaltic rocks [*Guo et al.*, 2007]. Abundant granulite xenoliths (see S1-2 in Figure 2) and xenocrysts in the basalts and the complex nature of the zircon populations (Table 1) indicate that the assimilation of older crustal components may have affected the chemistry of whole-rock samples, in particular the Ar content.

[21] Neogene alkaline magmatic rocks intruded into Tertiary sediments (including ultramafic-mafic volcanic rocks coexisting with carbonatites [*Yu*, 1994; *Yu et al.*, 2005]) are widespread in the Lixian area of Gansu Province, 300 km east of the Duofutun area (Figure 1b). The Lixian area is geologically a part of the west Qinling orogenic terrane, at the junction of the north China craton, the Yangtze craton, and the Tibetan Plateau. The occurrence of Neogene alkaline magmatism is consistent with late Cenozoic extension in north Tibet [*Yin et al.*, 1999]. The extension may be reflected in mantle-derived additions to the crust, relating the asthenospheric flow induced by the collision of the Indian plate with the Eurasian continent [i.e., *Niu*, 2005; *Mo et al.*, 2003].

5.2. Archean Crustal Remnants Beneath West Qinling

[22] Most of the zircon grains in the basalts are significantly older than the inferred eruption ages (~14 Ma) of the host rocks and therefore are xenocrysts. They may record the history of the unexposed deep lithosphere that the host magmas have passed through, or they may be recycled zircons derived from the Phanerozoic sedimentary strata in

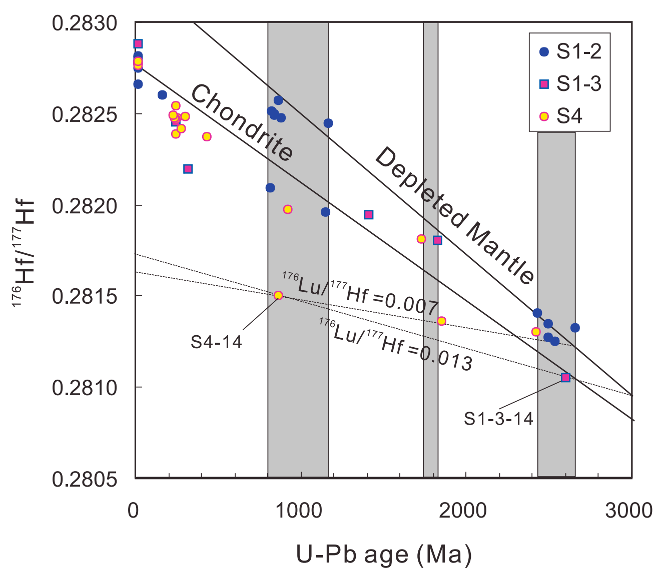

Figure 7. U-Pb age versus $^{176}Hf/^{177}Hf$ for zircons in the basalts from west Qinling. The shaded bands show periods of addition of juvenile materials in Neoarchean to early Paleoproterozoic and in Neoproterozoic times.

the Songpan-Ganzi area. It has become apparent in recent years that zircon xenocrysts can be entrained in variety of rocks, including basaltic to andesitic arc-related volcanics, ophiolitic basalts [*Hargrove et al.*, 2006; *Belyatevsky et al.*, 2008; *Bortnikov et al.*, 2008], and even ultramafic rocks [*Katayama et al.*, 2003; *Smith and Griffin*, 2005; *Zheng et al.*, 2006b, 2006c, 2008b]. Ancient xenocrysts in magma rocks intruding metamorphic terranes are often interpreted as being derived from anatectic melting of continental rocks or mixing of underplated magmas with old, lower crustal material. It is more difficult to explain zircon xenocrysts in mantle-derived rocks such as flood basalts and ophiolitic basalts because Zr is rarely saturated in such magmas. Some zircons may come directly from the mantle [*Tange and Takahashi*, 2004] because of the delamination of dense lower continental crust [*Kay and Kay*, 2003] or the contamination of the lithospheric mantle with "crustal" components during the migration of fluids/melts derived from the asthenosphere [*Griffin et al.*, 2004; *Zheng et al.*, 2006b] or from the dehydration of subducting lithosphere [*Katayama et al.*, 2003; *Smith and Griffin*, 2005; *Liou et al.*, 2007]. The whole-rock geochemistry of the basalts studied here [*Fan et al.*, 2007; *Guo et al.*, 2007] is not consistent with the assimilation of recycled crustal materials, i.e., the Songpan-Ganzi sedimentary rocks [*Zhao et al.*, 2008]. Therefore, the ancient xenocrystal zircons in these young basaltic rocks most probably are derived from the deep-seated lithosphere, such as the lower crust, represented by the granulite xenolith in sample S1-2 (see Figure 2a).

[23] Furthermore, U-Pb ages of >2.5 Ga for four grains (S1-2–52, S1-2–16, S1-2–26, and S1-3–14) from two samples indicate the presence of unexposed Archean crustal components beneath the west Qinling. Most of the Neoarchean zircons have positive $\varepsilon_{\mathrm{Hf}}$ (up to +8.5) and $T_{\mathrm{DM}} \approx 2.7$–2.5 Ga, reflecting new crustal growth at that time (see Figure 7). Some zircons with Neoarchean ages (i.e., 2603 ± 21 Ma in S1-3–14) have negative $\varepsilon_{\mathrm{Hf}}$; they record the existence of crustal materials older than 3.0 Ga.

[24] Detrital zircons extracted from flysch samples collected in the central part of the Songpan-Ganzi terrane, south of west Qinling (Figure 1b), also show abundant Neoarchean (~2.5–2.6 Ga) ages [*Bruguier et al.*, 1997; *Welslogel et al.*, 2006]. Deep seismic profiles [*Lu and Chen*, 1987; *Huang et al.*, 1992; *Zhu et al.*, 1995; *Cui et al.*, 1992, 1996; *Liu et al.*, 2006] across the west Qinling and the Songpan-Ganzi terranes apparently show that they are floored by continental basement [*Zhang*, 2001]. These data provide further evidence for the existence of Neoarchean rocks, containing Mesoarchean components, beneath west Qinling (Figure 7).

5.3. Post-Archean Thermal and Tectonic Modification

[25] The zircon grains in the basalts also record several important post-Archean thermal events,that may be related to the Proterozoic and Phanerozoic accretion or to reworking events that produced the uppermost crust of West Qinling.

[26] Three zircons with early Paleoproterozoic ages (~2425 Ma; S1-2–64, S1-2–65, and S4-32) have positive $\varepsilon_{\mathrm{Hf}}$ (2.4–6.2), showing the addition of juvenile material to the crust at this time. Three grains with late Paleoproterozoic ages (~1800 Ma; S1-3–2, S4-29, and S4-42) have a wide range of $\varepsilon_{\mathrm{Hf}}$ (−8.7 to +6.4) and thus high T_{DM} (2.0–2.6 Ga) and T_{crust} (2.1–3.1 Ga), indicating that this event involved thermal reworking of a heterogeneous older crust or mixing between crustally derived magmas and juvenile material.

[27] One concordant grain with a Mesoproterozoic age (i.e., ~1.4 Ga in S1-3–3) has positive $\varepsilon_{\mathrm{Hf}}$ (+2.0) and gives T_{DM} = 1.8 Ga and T_{crust} = 2.0 Ga, suggesting more reworking of the older crust at ~1.4 Ga. High values of $\varepsilon_{\mathrm{Hf}}$ (+14.2 in sample S1-2) in a 1163 Ma zircon are consistent with the addition of material derived from the depleted mantle, while low values of $\varepsilon_{\mathrm{Hf}}$ (−25.2 in sample S4) in a 868 Ma zircon suggest the remelting of Archean crustal materials (Figure 7).

[28] All Paleozoic (310 ± 10 Ma) and Mesozoic (230 Ma and 160 Ma) zircons have negative $\varepsilon_{\mathrm{Hf}}$ and 0.9–1.2 Ga T_{DM}; they may reflect the reworking of the crust accreted in Neoproterozoic time, with minor older (>1.5 Ga) components. The Neogene zircons have near-zero $\varepsilon_{\mathrm{Hf}}$ and 0.6–0.8 Ga T_{DM}, consistent with the remelting of Neoproterozoic crust.

5.4. Tectonic Affinity of West Qinling: North China or Yangtze Block?

[29] The Qinling orogen, connecting the north and south China blocks, is one of the most important tectonic belts in China and has been studied intensively [*Mattauer et al.*, 1985; *Zhang et al.*, 1995, 1996; *Meng and Zhang*, 1999]. The widespread outcrops of ultrahigh-pressure metamorphic rocks have ensured that much of the geology in the eastern Qinling-Sulu-Dabie orogen is well documented [*Xu et al.*, 1992; *Li et al.*, 1993; *Liou et al.*, 1989]. West Qinling is bounded along its northeast edge by the Qilian Shan (mountains) and to the southwest by the east Kunlun Shan (Figure 1a). The south-north trending Helan Shan lies to the north, and the Songpan-Ganzi terrane lies to the south. As the west Qinling segment acts as the northernmost part of the western Qinling-Songpan-Ganzi tectonic node [*Zhang et al.*, 2004], it has recently become the focus of much interest [*Yang et al.*, 2005; *Song et al.*, 2005; *Chen et al.*, 2008].

[30] Traditionally, it has been believed that the north China block was assembled in Archean time [*Liu et al.*, 1992; *Song et al.*, 1996; *Zheng et al.*, 2004a], while the Yangtze block was assembled during the Proterozoic [*Chen et al.*, 1998; *Ling et al.*, 2003] with minor Archean components [*Gao et al.*, 1999; *Qiu et al.*, 2000]. The Mesoproterozoic (1.4 Ga) and especially Neoproterozoic (~0.8 Ga) events were considered to distinguish the Yangtze block from the north China block [*Li et al.*, 2002; *Zheng and Zhang*, 2007]. However, with the accumulation of geochronological data, more and more components with Archean ages have been found in the Yangtze block [*Zheng et al.*, 2006a; *Zhang et al.*, 2006a and 2006b; *Liu et al.*, 2005]. At the same time, more evidence of Mesoproterozoic (~1.6–1.4 Ga [*Zhao et al.*, 2002; *Zheng et al.*, 2006b]) and Neoproterozoic (0.6–0.8 Ga [*Shao et al.*, 2002, 2005;

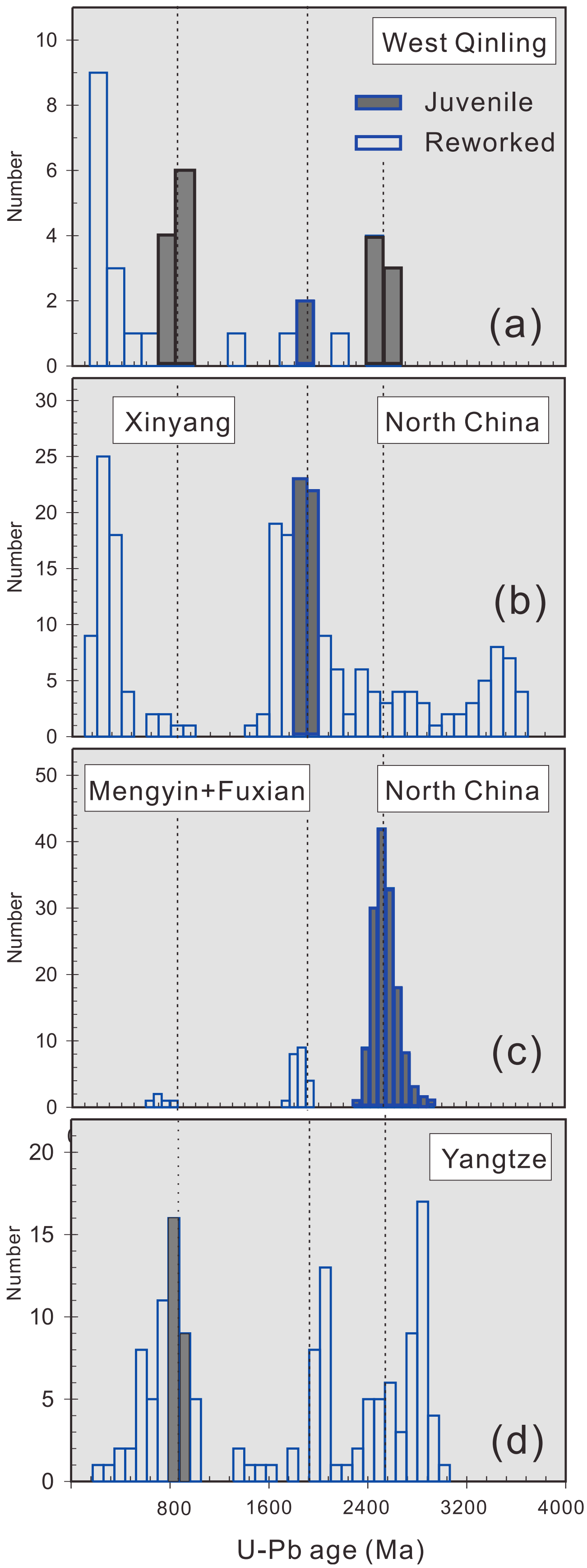

Yang et al., 2004; *Zheng et al.*, 2004b; *Yu et al.*, 2007]) magmatism has been recognized in the deep lithosphere of the north China block, making the distinction between the two blocks less clear cut.

[31] The pattern of thermal events beneath the Duofutun area in west Qinling, especially during Phanerozoic times (Figure 8a), is similar to that in Xinyang (Figure 8b), a locality at the southern margin of the north China block adjacent to the Qinling-Dabie-Sulu orogen (see XY in Figure 1a). In the Xinyang area, thermal events at ~440 Ma and ~230 Ma resulting from the northward subduction and collision of the Yangtze continent in both Paleozoic and early Mesozoic times were clearly recorded in the lowermost crust by zircons from eclogite and high-pressure mafic granulite and from the lithospheric upper mantle [*Zheng et al.*, 2006c, 2008b], respectively. The thermal event related to subsequent lithospheric extension resulting from asthenospheric upwelling in Jurassic time (~160 Ma) also affected the lowermost crust [*Zheng et al.*, 2008b]. West Qinling is contiguous with east Qinling, which contains both the north and south Qinling subbelts. The studied area appears to be located in the northern part of the west Qinling block and so could as easily be contiguous with north Qinling as with south Qinling, which is geologically similar to the Yangtze block [*Zhang et al.*, 1994, 1995; *Zhou and Graham*, 1996; *Meng and Zhang*, 2000; *Chinese Geological Society*, 2004; *Weislogel*, 2008]. Up to 50% of the Permo-Triassic clastic sedimentary rocks of west Qinling also contain material derived from the basement rocks on the north China block [*Chen et al.*, 2008]. On the other hand, work by *Weislogel et al.* [2006] and *Garzione et al.* [2004] also documents the presence of abundant recycled material in the Mesozoic strata of the Songpan-Ganzi, with an interpreted north China provenance. Therefore, we interpret west Qinling, the northernmost part of the western Qinling-Songpan-Ganzi terrane, as part of the southern margin of the north China block (i.e., north Qinling), rather than the slightly more distant Yangtze block (i.e., south Qinling).

[32] The addition of significant asthenosphere-derived material to the west Qinling terrane at 1.1–0.8 Ga and 2.7–2.4 Ga (Figure 7) also resulted in reworking of older crustal volumes. The recorded events also coincide with the peaks for thermal events in the Yangtze block in the Neoproterozoic [*Li et al.*, 2002; *Zheng et al.*, 2006a; *Zheng and Zhang*, 2007] and with those in the interior (Mengyin and Fuxian) of the north China block in the Neoarchean-early Paleoproterozoic (see MY and FX in Figure 8c). The correspondence shows the possible tectonic affinities of the west Qinling terrane with the

Figure 8. Histograms of for concordant and nearly concordant U-Pb ages of zircons in the Duofutun basaltic rocks showing source type (reworked or juvenile) as derived from Hf isotope data. Similar xenocrystal data from the Xinyang [*Zheng et al.*, 2004a, 2006c, 2008b] and Mengyin and Fuxian [2004b, 2009] localities, located at the southern margin and interior of the north China block and the Yangtze block (including Jingshan, Ningxiang, and Zhenyuan [*Zheng et al.*, 2006a]) are shown for comparison, respectively.

Yangtze block in the Neoproterozoic (Figure 8d) and with the north China block in the Neoarchean-early Paleoproterozoic. Therefore, we interpret the west Qinling orogenic terrane as a microcontinental block that originally separated from the north China block close to the northern Yangtze block during the Meso-Neoproterozoic. This microcontinent then redocked with the southern margin of the north China block in the Phanerozoic and was finally affected by the northward subduction and collision of the Yangtze block in the Paleozoic and early Mesozoic.

6. Conclusions

[33] Neogene (~14 Ma) basaltic magmatism has occurred in west Qinling, at the northeastern corner of the Tibetan Plateau. Furthermore, U-Pb ages and Hf isotopic data of xenocrystic zircons indicate that the unexposed Neoarchean (2.7–2.5 Ga) basement beneath the Phanerozoic outcrops in west Qinling has affinities with the southern margin of the north China block. The basement has a complex evolution, including the addition of juvenile mantle material at ~2.7–2.4 Ga and 1.1–0.8 Ga and reworking at ~1.8 Ga and possibly at 1.4 Ga. Phanerozoic thermal events at 320–300 Ma, 230 Ma, and 160 Ma also have affected the basement. We interpret the west Qinling orogenic terrane as originally separated from the north China block, joined to the northern Yangtze block during the Meso-Neoproterozoic, and finally involved in the northward subduction and collision of the Yangtze block in the Paleozoic and early Mesozoic and subsequent lithospheric extension in the Jurassic.

[34] **Acknowledgments.** The authors thank Onno Oncken, Lothar Ratschbacher, Alfred Kroener, and an anonymous reviewer for their comments and suggestions, which improved the manuscript significantly. This study was supported by the Chinese National Natural Science Foundation (90714002, 40821061, and 40673002) and "973" project (2006CB403502), ARC Discovery Projects, and Linkage International grants (S.Y.O. and W. L.G.), a Hong Kong University CRCG Grant (M.S.) and the Sino-British Fellowship Trust for the first author's 3 month visit to Hong Kong University during 2007-2008. Analytical data were obtained using instrumentation funded by ARC LIEF, DEST Systemic Infrastructure grants, Macquarie University, and industry. This is contribution 617 from the ARC National Key Centre for the Geochemical Evolution and Metallogeny of Continents (http://www.gemoc.es.mq.edu.au).

References

Andersen, T. (2002), Correction of common lead in U-Pb analyses that do not report ^{204}Pb, *Chem. Geol.*, *192*, 59–79, doi:10.1016/S0009-2541(02)00195-X.

Belousova, E. A., W. L. Griffin, S. R. Shee, S. E. Jackson, and S. Y. O'Reilly (2001), Two age populations of zircons from the Timber Creek kimberlites, Northern Territory, Australia as determined by laser ablation ICPMS analysis, Aust. *J. Earth Sci.*, *48*, 756–766.

Belyatevsky, B., E. Lepekhina, A. Antonov, O. Shuliatin, and S. Sergeev (2008), Age and genesis of accessory zircon from MAR gabbroids, *Geophys. Res. Abstr.*, *10*, EGU2008-A-01314.

Blichert-Toft, J., and F. Albarède (1997), The Lu-Hf geochemistry of chondrites and evolution of the mantle-crust system, *Earth Planet. Sci. Lett.*, *148*, 243–258, doi:10.1016/S0012-821X(97)00040-X.

Bortnikov, N. S., T. F. Zinger, E. N. Lepekhina, A. V. Antonov, and S. A. Sergeev (2008), Cenozoic and Precambrian accessory zircons in gabbroids of the third layer of oceanic crust in axial part of the mid-Atlantic ridge, 6°N: U-Pb SIMS SHRIMP data, *Eos Trans. AGU*, *89*(53), Fall Meet. Suppl., Abstract V41D-2111.

Bruguier, O., J. R. Lancelot, and J. Malavieille (1997), U-Pb dating on single detrital zircon grains from the Triassic Songpan-Ganze flysch (central China): Provenance and tectonic correlations, *Earth Planet. Sci. Lett.*, *152*, 217–231, doi:10.1016/S0012-821X(97)00138-6.

Chen, J. F., and B. M. Jahn (1998), Crustal evolution of southeastern China: Nd and Sr isotopic evidence, *Tectonophysics*, *284*, 101–133, doi:10.1016/S0040-1951(97)00186-8.

Chen, Y. L., D. P. Li, J. Zhou, H. F. Zhang, F. Liu, L. S. Nie, L. T. Jiang, and X. M. Liu (2008), U-Pb ages of zircons in western Qinling Shan, China, and their tectonic implications, *Earth Sci. Front*, *15*(4), 88–107, doi:10.1016/S1872-5791(08)60042-1.

Chinese Geological Society (2004), *Geological Map of the People's Republic of China Explanatory Notes*, Sino Map Press, Beijing.

Cui, Z., Z. Yin, E. Gao, D. Lu, and W. Fu (1992), Yadong-Golmud GGT. Velocity Structure and Deep-Seated Structure of the Qinghai-Xizang (Tibet) Plateau (in Chinese), *Geol. Mem., Ser. 5*, *15*, 112 pp.

Cui, Z., Y. Sun, and X. R. Wang (1995), Discovery of radiolarians from the Danfeng ophiolite zone, North Qinling, and their geological significance, *Chin. Sci. Bull.*, *40*, 1686–1688.

Cui, Z., J. Chen, and L. Wu (1996), Altay-Taiwan GGT: Texture and Structure of Huashixia-Shaoyang Deep Crust (in Chinese), *Geol. Mem., Ser. 5*, *21*, 48 pp.

Debièvre, P., and P. D. P. Taylor (1993), Table of the isotopic composition of the elements, *Int. J. Mass Spectrom. Ion Process.*, *123*, 149–166, doi:10.1016/0168-1176(93)87009-H.

Enkin, R. J., Z. Y. Yang, Y. Chen, and V. Courtillot (1992), Paleomagnetic constraints on the geodynamic history of the major blocks of China from the Permian to the present, *J. Geophys. Res.*, *97*, 13,953–13,989, doi:10.1029/92JB00648.

Fan, L. Y., Y. J. Wang, and X. Y. Li (2007), Geochemical characteristics of late Mesozoic mafic volcanic rocks from western Qinling and its tectonic implications (in Chinese), *J. Mineral. Petrol. Econ. Geol.*, *27*(3), 63–72.

Feng, Y. M., X. Z. Cao, and E. P. Zhang (2003), Geological evolution of the western Qinling orogen (in Chinese), *Northwest Geol.*, *36*(1), 1210–1214.

Gao, S., W. L. Ling, Y. M. Qiu, L. Zhou, G. Hartmann, and K. Simon (1999), Contrasting geochemical and Sm-Nd isotopic compositions of Archean metasediments from the Kongling high-grade terrain of the Yangtze craton: Evidence for cratonic evolution and redistribution of REE during crustal anatexis, *Geochim. Cosmochim. Acta*, *63*, 2071–2088, doi:10.1016/S0016-7037(99)00153-2.

Garzione, C. N., L. Dettman, and B. K. Horton (2004), Carbonate oxygen isotope paleoaltimetry: Evaluating the effect of diagenesis on paleoelevation estimates for the Tibetan plateau, *Palaeogeogr. Palaeoclimatol. Palaeoecol.*, *212*, 119–140.

Griffin, W. L., N. J. Pearson, E. Belousova, S. E. Jackson, S. Y. O'Reilly, E. van Achterberg, and S. R. Shee (2000), The Hf isotope composition of cratonic mantle: LAM-MC-ICPMS analysis of zircon megacrysts in kimberlites, *Geochim. Cosmochim. Acta*, *64*, 133–147, doi:10.1016/S0016-7037(99)00343-9.

Griffin, W. L., X. Wang, S. E. Jackson, N. J. Pearson, S. Y. O'Reilly, X. S. Xu, and X. M. Zhou (2002), Zircon chemistry and magma mixing: SE China; in-situ analysis of Hf isotopes, Tonglu and Pingtan igneous complex, *Lithos*, *61*, 237–269, doi:10.1016/S0024-4937(02)00082-8.

Griffin, W. L., E. A. Belousova, S. R. Shee, N. J. Pearson, and S. Y. O'Reilly (2004), Archean crustal evolution in the northern Yilgarn Craton: U-Pb and Hf-isotope evidence from detrital zircons, *Precambrian Res.*, *131*, 231–282, doi:10.1016/j.precamres.2003.12.011.

Griffin, W. L., W. J. Powell, N. J. Pearson, and S. Y. O'Reilly (2008), GLITTER: Data reduction software for laser ablation ICP-MS, in *Laser Ablation-ICP-MS in the Earth Sciences*, *Mineralogical Association of Canada Short Course Series*, vol. 40, appendix 2, edited by P. Sylvester, pp. 204–207, Mineralogical Association of Canada, Toronto.

Guo, A. L., G. W. Zhang, Y. G. Sun, and S. Y. Cheng (2007), Tertiary Duofuton Na-rich mafic volcanic rocks, on northeastern margin of the Qinghai-Tibet Plateau and their tectonic implications (in Chinese with English abstract), *Earth Sci. Front*, *14*(3), 73–83.

Hacker, B. R., L. Ratschbacher, and J. G. Liou (2004), Subduction, collision and exhumation in the ultra-high-pressure Qinling-Dabie orogen, in *Aspects of the Tectonic Evolution of China*, *Geol. Soc. London Spec. Publ.*, *226*, 157–175.

Hargrove, U. S., R. J. Stern, J. I. Kimura, W. I. Manton, and P. R. Johnson (2006), How juvenile is the Arabian-Nubian Shield? Evidence from Nd isotopes and pre-Neoproterozoic inherited zircon in the Bi'r Umq suture zone, Saudi Arabia, *Earth Planet Sci. Lett.*, *252*, 308–326.

Hermann, J., and D. H. Green (2001), Experimental constraints on high pressure melting in subducted crust, *Earth Planet. Sci. Lett.*, *188*, 149–168, doi:10.1016/S0012-821X(01)00321-1.

Huang, L., G. Li, E. Gao, S. Wang, and Z. Cui (1992), Characteristics of the Structure and Velocity Distribution of Crust in Xizang (Tibet) Plateau (in Chinese), *Geol. Mem., Ser. 5*, *10*, 122 pp.

Jackson, S. E., N. J. Pearson, W. L. Griffin, and E. A. Belousova (2004), The application of laser ablation-inductively coupled plasma-mass spectrometry to in situ U-Pb zircon geochronology, *Chem. Geol.*, *211*, 47–69, doi:10.1016/j.chemgeo.2004.06.017.

Kay, R. W., and S. M. Kay (1993), Delamination and delamination magmatism, *Tectonophysics*, *219*, 177–189, doi:10.1016/0040-1951(93)90295-U.

Kröener, A., G. W. Zhang, and Y. Sun (1993), Granulites in the Tongbai area,Qinling Belt, China: Geochemistry, petrology, single zircon geochronology, and implications for the tectonic evolution of eastern Asia, *Tectonics*, *12*(1), 245–256, doi:10.1029/92TC01788.

Lai, X., H. Yin, and F. Yang (1992), The character and evolution of ecostratigraphy and paleobiogeography of Triassic Qinling basin, *Earth Sci. J. China Univ. Geosci.*, *17*(3), 345–352.

Lerch, M. F., F. Xue, A. Kroëner, G. W. Zhang, and W. Tod (1995), A Middle Silurian-Early Devonian magmatic arc in the Qinling Mountains of central China, *J. Geol.*, *103*(4), 437–449, doi:10.1086/629762.

Li, S. G., et al. (1993), Collision of the North China and Yangtze Blocks and formation of coesite-bearing eclogites: Timing and processes, *Chem. Geol.*, *109*, 89–111, doi:10.1016/0009-2541(93)90063-O.

Li, Z. X., X. H. Li, H. W. Zhou, and P. D. Kinny (2002), Grevillian continental collision in south China: New SHRIMP U-Pb zircon results and implications for the configuration of Rodinia, *Geology*, *30*, 163–166, doi:10.1130/0091-7613(2002)030<0163:GCCISC>2.0.CO;2.

Ling, W. L., S. Gao, B. R. Zhang, H. M. Li, Y. Liu, and J. P. Chen (2003), Neoproterozoic tectonic evolution of the northwestern Yangtze craton, South China: Implications for amalgamation and break-up of the Rodinia Supercontinent, *Precambrian Res.*, *122*, 111–140, doi:10.1016/S0301-9268(02)00222-X.

Liou, J. G., S. A. Graham, and S. Maruyama (1989), Proterozoic blueschist belt in Western China: Best documented Precambrian blueschists in the world, *Geology*, *17*, 1127–1131, doi:10.1130/0091-7613(1989)017<1127:PBBIWC>2.3.CO;2.

Liou, J. G., R. Y. Zhang, and W. G. Ernst (2007), Very high-pressure orogenic garnet peridotites, *Proc. Natl. Acad. Sci. U. S. A.*, *104*, 9116–9121, doi:10.1073/pnas.0607300104.

Liu, D. Y., A. P. Nutman, W. Compston, J. S. Wu, and Q. H. Shen (1992), Remnants of 3800 Ma crust in Chinese part of the Sino-Korean craton, *Geology*, *20*, 339–342, doi:10.1130/0091-7613(1992)020<0339:ROMCIT>2.3.CO;2.

Liu, M. J., W. D. Mooney, S. L. Li, N. Okaya, and S. Detweiler (2006), Crustal structure of the northeastern margin of the Tibetan plateau from the Songpan-Ganzi terrane to the Ordos basin, *Tectonophysics*, *420*, 253–266, doi:10.1016/j.tecto.2006.01.025.

Liu, X. M., S. Gao, and W. L. Ling (2005), The discovery of 3.5 Ga detrital zircons in the Yangtze craton and its geological implications, *Prog. Nat. Sci.*, *15*(11), 1334–1337.

Lu, D. Y., and J. P. Chen (1987), The deep crustal structure of the Tuotuohe-Golumd area, north Tibet (in Chinese), *Geol. Rev.*, *33*, 125–135.

Ludwig, K. R. (2000), *Isoplot—A Geochronological Toolkit for Microsoft Excel*, *Spec Publ. 1a*, *53*, Berkeley Geochronol. Cent., Berkeley, Calif.

Mattauer, M., et al. (1985), Tectonics of the Qinling belt: Build-up and evolution of eastern Asia, *Nature*, *317*, 496–500, doi:10.1038/317496a0.

Meng, Q. R., and G. W. Zhang (1999), Timing of collision of the North and South China blocks: Controversy and reconciliation, *Geology*, *27*(2), 123–126, doi:10.1130/0091-7613(1999)027<0123:TOCOTN>2.3.CO;2.

Meng, Q. R., and G. W. Zhang (2000), Geologic framework and tectonic evolution of the Qinling orogen, central China, *Tectonophysics*, *323*, 183–196, doi:10.1016/S0040-1951(00)00106-2.

Mo, X. X., Z. D. Zhao, J. F. Deng, G. C. Dong, S. Zhou, T. Y. Guo, S. Q. Zhang, and L. L. Wang (2003), Response of volcanism to the India-Asian collision, *Earth Sci. Front*, *10*, 135–148.

Niu, Y. L. (2005), Generation and evolution of basaltic magmas: Some basic concepts and a new view on the origin of Mesozoic-Cenozoic basaltic volcanism in Eastern China (in Chinese with English abstract), *Geol. J. China Univ.*, *11*, 9–46.

Qiu, Y. M., S. Gao, N. J. McNaughton, D. I. Groves, and W. L. Ling (2000), First evidence of >3.2 Ga continental crust in the Yangtze craton of south China and its implications for Archean crustal evolution and Phanerozoic tectonics, *Geology*, *28*, 11–14, doi:10.1130/0091-7613(2000)028<0011:FEOGCC>2.0.CO;2.

Ratschbacher, L., B. R. Hacker, and A. Calvert (2003), Tectonics of the Qinling (Central China): Tectonostratigraphy, geochronology, and deformation history, *Tectonophysics*, *366*, 1–53, doi:10.1016/S0040-1951(03)00053-2.

Shao, J. A., L. Q. Zhang, and D. M. Li (2002), Three Proterozoic extensional events in North China Craton (in Chinese), *Acta Petrol. Sin.*, *18*(2), 152–160.

Shao, J. A., M. G. Zhai, and L. Q. Zhang (2005), Identification of five time-groups of dike swarms in Shanxi-Hebei-Inner Mongulia border area and its tectonic implications (in Chinese with English abstract), *Acta Geol. Gansu*, *79*(1), 56–67.

Smith, D., and W. L. Griffin (2005), Navajo garnetites and rock-water interactions in the mantle below the Colorado Plateau, southwestern United States, *J. Petrol.*, *46*, 1901–1924, doi:10.1093/petrology/egi042.

Song, B., A. P. Nutman, D. Y. Liu, and J. S. Wu (1996), 3800 to 2500 Ma crustal evolution in the Anshan area of Liaoning Province, northeastern China, *Precambrian Res.*, *78*, 79–94, doi:10.1016/0301-9268(95)00070-4.

Song, S. G., L. F. Zhang, Y. L. Niu, L. Su, P. Jian, and D. Y. Liu (2005), Geochronology of diamond-bearing zircons from garnet peridotite in the North Qaidam UHPM belt, northern Tibetan Plateau: A record of complex histories from oceanic lithosphere subduction to continental collision, *Earth Planet. Sci. Lett.*, *234*, 99–118, doi:10.1016/j.epsl.2005.02.036.

Sun, W., I. S. Williams, and S. Li (2002), Carboniferous and Triassic eclogites in the western Dabie Mountains, east-central China: Evidence for protracted convergence of the North and South China blocks, *J. Metamorph. Geol.*, *20*, 873–886, doi:10.1046/j.1525-1314.2002.00418.x.

Tange, Y., and E. Takahashi (2004), Stability of the high-pressure polymorph of zircon (ZrSiO4) in the deep mantle, *Phys. Earth Planet. Inter.*, *143–144*, 223–229, doi:10.1016/j.pepi.2003.10.009.

Weislogel, A. L. (2008), Tectonostratigraphic and geochronologic constraints on evolution of the northeast Paleotethys from the Songpan-Ganzi complex, central China, *Tectonophysics*, *451*, 331–345, doi:10.1016/j.tecto.2007.11.053.

Weislogel, A. L., S. A. Graham, E. Z. Chang, J. L. Wooden, G. E. Gehreis, and H. S. Yang (2006), Detrial zircon provenance of the Late Triassic Songpan-Ganzi complex: Sedimentary record of collision of the north and south China blocks, *Geology*, *34*, 97–100, doi:10.1130/G21929.1.

Xu, S. T., A. I. Okay, S. Ji, A. M. C. Sengor, Y. Kiu, and L. Jiang (1992), Diamond from the Dabie Shan metamorphic rocks and its implication for tectonic setting, *Science*, *256*, 80–92, doi:10.1126/science.256.5053.80.

Xue, F., M. F. Lerch, and A. Kröner (1996), Tectonic evolution of the East Qinling Mountains, China, in Paleozoic: A review on new tectonic model, *Tectonophysics*, *253*, 271–284, doi:10.1016/0040-1951(95)00060-7.

Yang, J. H., F. Y. Wu, and Y. B. Zhang (2004), Identification of Neoproterozoic zircons in a Triassic dolerite from the Liaodong Peninsula, northeast China, *Chin. Sci. Bull.*, *49*(18), 1958–1962, doi:10.1360/04wd0248.

Yang, J. S., F. L. Liu, C. L. Wu, Z. Q. Xu, and R. D. Shi (2005), Two ultrahigh-pressure metamorphic events recognized in the central orogenic belt of China: Evidence from the U-Pb dating of coesite-bearing zircons, *Int. Geol. Rev.*, *47*, 327–343, doi:10.2747/0020-6814.47.4.327.

Yin, A., and S. Nie (1996), A Phanerozoic palinspastic reconstruction of China and its neighboring regions, in *The Tectonics of Asia*, edited by A. Yin and T. M. Harrison, pp. 442–485, Cambridge Univ. Press, New York.

Yin, A., P. A. Kapp, M. A. Murphy, C. E. Manning, and T. M. Harrison (1999), Evidence for significant Late Cenozoic E-W extension in North Tibet, *Geology*, *27*, 787–790, doi:10.1130/0091-7613(1999)027<0787:SLNEWE>2.3.CO;2.

Yu, C. M., J. P. Zheng, and W. L. Griffin (2007), In situ Re-Os isotope ages of sulfides in Hannuoba peridotitic xenoliths: Significance for the frequently occurring mantle events beneath the North China Block, *Chin. Sci. Bull.*, *52*, 2847–2853, doi:10.1007/s11434-007-0354-2.

Yu, X. H. (1994), Cenozoic potassic alkaline ultrabasic volcanic rocks and its genesis in Lixian-Dangchang area, Gansu Province (in Chinese), *Tethyan Geol.*, *18*, 114–129.

Yu, X. H., Z. D. Zhao, X. X. Mo, S. Zhou, D. Q. Zhu, and Y. L. Wang (2005), ^{40}Ar/^{39}Ar dating for Cenozoic kamafugites from western Qinling in Gansu Province, *Chin. Sci. Bull., 50*(21), 2638–2643.

Zhai, X. M., H. W. Day, and B. R. Hacker (1998), Paleozoic metamorphism in the Qinling orogen, Tongbai Mountains, central China, *Geology*, *26*, 371–374, doi:10.1130/0091-7613(1998)026<0371:PMITQO>2.3.CO;2.

Zhang, B., T. Luo, S. Gao, J. Ouyang, Y. Han, and C. Gao (1994), Geochemical constraints on the evolution of North China and Yangtze blocks, *J. Asian Earth Sci.*, *9*, 405–416, doi:10.1016/0743-9547(94)90052-3.

Zhang, G. W., Q. R. Meng, and S. C. Lai (1995), Tectonics and structures of the Qinling orogenic belt, *Sci. China*, *38*, 1379–1386.

Zhang, G. W., Q. R. Meng, and Z. P. Yu (1996), Orogenic processes and dynamics of the Qinling, *Sci. China, Ser. D*, *39*, 225–234.

Zhang, G. W., A. L. Guo, and A. P. Yao (2004), Western Qinling-Songpan continental tectonic node in China's continental tectonics, *Earth Sci. Front*, *11*(3), 23–32.

Zhang, H. F., S. Gao, B. R. Zhang, T. C. Luo, and W. L. Lin (1997), Pb isotopes of granitoids suggest Devonian accretion of Yangtze (south China) craton to north China craton, *Geology*, *25*, 1015–1018, doi:10.1130/0091-7613(1997)025<1015:PIOGSD>2.3.CO;2.

Zhang, K. J. (2001), Is the Songpan-Garze terrane (central China) really underlain by oceanic crust? *J. Geol. Soc. India*, *57*, 223–230.

Zhang, S. B., Y. F. Zheng, Y. B. Wu, Z. F. Zhao, S. Gao, and F. Y. Wu (2006a), Zircon isotope evidence for ≥3.5 Ga continental crust in the Yangtze craton of China, *Precambrian Res.*, *146*, 16–34, doi:10.1016/j.precamres.2006.01.002.

Zhang, S. B., Y. F. Zheng, Y. B. Wu, Z. F. Zhao, S. Gao, and F. Y. Wu (2006b), Zircon U-Pb age and Hf-O isotope evidence for Paleoproterozoic metamorphic event in South China, *Precambrian Res.*, *151*, 265–288, doi:10.1016/j.precamres.2006.08.009.

Zhao, T. P., M. F. Zhou, M. G. Zhai, and B. Xia (2002), Paleoproterozoic rifting-related volcanism of the Xiong'er Group, north China craton: Implications for the breakup of Columbia, *Int. Geol. Rev.*, *44*, 336–351, doi:10.2747/0020-6814.44.4.336.

Zhao, W. T., X. H. Yu, M. Liu, Z. D. Zhao, and X. X. Mo (2008), Clinopyroxene in the late Mesozoic igneous rocks of the northeastern part of the Tibetan Plateau and its implication, *Bull. Mineral. Petrol. Geochem.*, *27*, 289–292.

Zheng, J. P., W. L. Griffin, S. Y. O'Reilly, F. X. Lu, C. Y. Wang, M. Zhang, F. Z. Wang, and H. M. Li (2004a), 3.6 Ga lower crust in central China: New evidence on the assembly of the North China Craton, *Geology*, *32*, 229–232, doi:10.1130/G20133.1.

Zheng, J. P., W. L. Griffin, S. Y. O'Reilly, F. X. Lu, and C. M. Yu (2004b), U-Pb and Hf- Isotope analysis of zircons in mafic xenoliths from Fuxian kimberlites: Evolution of the lower crust beneath the

North China Craton, *Contrib. Mineral. Petrol.*, *148*, 79–103, doi:10.1007/s00410-004-0587-x.

Zheng, J. P., W. L. Griffin, S. Y. O'Reilly, M. Zhang, N. Pearson, and Y. M. Pan (2006a), Widespread Archean basement beneath the Yangtze Craton, *Geology*, *34*, 417–420, doi:10.1130/G22282.1.

Zheng, J. P., W. L. Griffin, S. Y. O'Reilly, J. S. Yang, and R. Y. Zhang (2006b), A refractory mantle protolith in younger continental crust, east-central China: Age and composition of zircon in the Sulu UHP peridotite, *Geology*, *34*, 705–708, doi:10.1130/G22569.1.

Zheng, J. P., W. L. Griffin, S. Y. O'Reilly, M. Zhang, and N. Pearson (2006c), Zircons in mantle xenoliths record the Triassic Yangtze-North China continental collision, *Earth Planet. Sci. Lett.*, *247*, 130–142, doi:10.1016/j.epsl.2006.05.011.

Zheng, J. P., W. L. Griffin, H. Y. Tang, Z. H. Zhang, Y. P. Su, and G. L. Liu (2008a), Archean basement similar to the North China and Yangtze continents may be existed beneath the western Cathaysia (in Chinese with English abstract), *Geol. J. China Univ.*, *14*, 549–557.

Zheng, J. P., W. L. Griffin, S. Y. O'Reilly, B. Q. Hu, M. Zhang, N. Pearson, F. Z. Wang, and F. X. Lu (2008b), Continental collision/accretion and modification recorded in the deep lithosphere of central China, *Earth Planet. Sci. Lett.*, *269*, 497–506, doi:10.1016/j.epsl.2008.03.003.

Zheng, J. P., W. L. Griffin, S. Y. O'Reilly, G. L. Liu, N. Pearson, M. Zhang, C. M. Yu, Y. P. Su, and H. Y. Tang (2009), Neoarchean (2.7–2.8 Ga) accretion beneath the north China Craton: U-Pb age, trace elements and Lu-Hf isotopes of zircons in diamondiferous kimberlites, *Lithos*, *112*, 188–202.

Zheng, Y. F., and S. B. Zhang (2007), Formation and evolution of Precambrian continental crust in South China, *Chin. Sci. Bull.*, *52*(1), 1–12, doi:10.1007/s11434-007-0015-5.

Zhou, D., and S. A. Graham (1996), Extrusion of the Altyn Tagh wedge: A kinematic model for the Altyn Tagh fault and palinspastic reconstruction of northern China, *Geology*, *24*, 427–430, doi:10.1130/0091-7613(1996)024<0427:EOTATW>2.3.CO;2.

Zhu, L., T. J. Owens, and G. E. Randall (1995), Lateral variation in crustal structure of the northern Tibetan Plateau inferred from tele-seismic receiver foundations, *Bull. Seismol. Soc. Am.*, *85*, 1531–1540.

W. L. Griffin and S. Y. O'Reilly, Australian Research Council National Key Centre for Geochemical Evolution and Metallogeny of Continents, Department of Earth and Planetary Sciences, Macquarie University, Sydney, NSW 2109, Australia.

M. Sun, Department of Earth Sciences, University of Hong Kong, Pokfulam Road, Hong Kong, China.

H. Y. Tang, L. Xiao, H. F. Zhang, Z. H. Zhang, J. P. Zheng, and H. W. Zhou, State Key Laboratory of Geological Processes and Mineral Resources, China University of Geosciences, Wuhan 430074, China. (jpzheng@cug.edu.cn; jpzheng2003@yahoo.com)